July 14, 2011
Report No. E11-225

Ductless Heat Pump Impact & Process Evaluation: Lab-Testing Report

Prepared by:
Ecotope Inc.
4056 9th Avenue NE
Seattle, WA 98105

Northwest Energy Efficiency Alliance
PHONE
503-688-5400
FAX
503-688-5447
EMAIL
info@neea.org

Table of Contents

List of Tables

List of Figures

Executive Summary

NEEA hired the team of Ecotope, Inc., supported by Research Into Action, Inc., Stellar Processes, and Herrick Labs, to evaluate the Northwest Ductless Heat Pump Pilot Project. The pilot project ran from October 2008 to December 2009. The DHP Pilot Project sought to displace energy used by zonal electric heating equipment, with DHPs. The DHP Program, which succeeded the pilot project in 2010, continues to address this goal.

As an integral part of the Ductless Heat Pump Evaluation Project, Ecotope carried out an extensive laboratory analysis of DHP performance. The lab evaluation developed a detailed understanding of DHP performance to support the field monitoring and subsequent data analysis of DHPs installed in houses. The evaluation also collected data for creating detailed and accurate equipment performance models for use in simulation tools.

In conjunction with NEEA, Ecotope established the following goals for the lab evaluation:

- Develop a performance map of the equipment at all temperature bins and operating modes while providing special focus to low temperature heating performance.
- Review standard ratings (AHRI 210/240) published by the manufactures and establish the relationship between the ratings at controlled test conditions and other tests at conditions more likely in the Pacific Northwest applications.
- Assess performance variation with various control strategies and operating modes.
- Conduct measurements to review and verify the data collected in the field metering, especially in situ coefficient of performance (COP) measurements. Ecotope installed a detailed metering package in over 30 houses to directly measure equipment output capacity and input power to observe COP (the details of which will be presented in another report).
- Establish empirical performance curves to predict the efficiency and output of the equipment in energy simulations and other engineering calculations. The modeling capability will directly support regional energy planning efforts and conservation program design.

Working with NEEA, Ecotope selected two DHP models to evaluate which are representative of those found in the field installations: the Fujitsu 12RLS and Mitsubishi FE12NA. Ecotope developed a testing strategy and contracted with Herrick Labs of Purdue University to conduct the measurements. The lab measured performance impacts on the two equipment models over a wide range of operating conditions that would be encountered in Pacific Northwest installations, including outside temperature ranges from -5°F to +105°F. Additionally, because the efficiency and flexibility of the DHP systems stem from their ability to vary compressor thermal outputs and indoor fan flow in response to changing ambient conditions or occupant intervention, the testing plan also called for measuring high, medium, and low capacity outputs and also included high, medium, and low indoor fan speeds.

Herrick Labs installed all necessary instrumentation to accurately and precisely measure the DHP operating parameters for all the data points in the testing plan. In particular, the lab

measured both an air-side and refrigerant-side equipment output capacity. These measurements are two independent measurements of the same quantities. The agreement achieved between the two measurements was 6% or less for both equipment models in both heating and cooling modes. The agreement demonstrates the veracity of the data.

Using the data on the equipment performance map collected in the lab tests, both Ecotope and Herrick Labs developed predictive energy use models of the equipment. Ecotope's model will be used inside the SEEM (Simple Energy and Enthalpy Model) residential energy use simulation to predict annual energy consumption and savings from DHP installations. The field data collected from installations across the region will be integrated with the laboratory test data and results to refine, calibrate, and validate the model.

The detailed performance mapping and subsequent analysis produced significant findings including:

- **The lab data demonstrates the high performance of both models.** The highly efficient operation will enable significant energy savings opportunities in both retrofit and new applications. Both equipment models have the potential to deliver on the promise of generous energy savings. Had the lab data revealed poor efficiency results, the ultimate energy savings estimates would be compromised. In the end, the savings achieved in a particular house will depend on a number of factors including the installation location within the building or the interaction with the existing heating system. Compressor and distribution efficiency of the DHP, however, will provide a strong foundation on which to build energy savings.

- **Lab and field COP measurements show good agreement.** The early analysis of the field data compares well to the lab measurements. Both measurements provide a useful cross reference for each other. The lab data is collected in a stable, repeatable, and highly controllable situation which provides a "reference set" for the field measurements of similar DHPs. Likewise, the field metering of COP shows which equipment operating modes are most common and therefore the most important parameters to measure in the lab. At the outset of the project, Ecotope did not anticipate the amount of synergy between the two data sets. It yields more confidence in both, while simultaneously demonstrating the benefits of an integrated evaluation approach to ductless heat pumps.

- **Both equipment models perform well at low outdoor temperatures.** Both models continue to operate well in cold temperatures with the 12RLS showing slightly higher capacity and efficiency. Installers and home-owners should be made aware that the equipment will continue to run and provide benefits at cold temperatures so that energy savings can be maximized.

- **The current HSPF and SEER ratings are not well suited to DHPs.** The testing standard and calculation procedure do not always produce ratings which characterize the performance of the equipment well or allow one to determine how the equipment might operate in a controlled lab environment, let alone a field installation. In lieu of the ratings, more data is needed to assess both the relative performance between models and the likely energy use of a single model. Performance curves (including capacity and input power over a range of compressor loadings) and descriptions of operational

strategies will be useful in this regard. An updated testing procedure should include changes to the testing conditions, compressor speeds in particular, that make them more applicable to the way the DHPs perform in actual operation.

- **The equipment can be modeled in SEEM.** The performance model developed with the data collected in the lab will be implemented within SEEM. The models will be carefully calibrated with field data to provide accurate predictive capacity. The simulation will be appropriate to determine energy savings in both retrofit applications and new construction scenarios. This will allow the results of the lab testing and field data to be generalized to future evaluation of DHPs as a regional energy efficiency resource.

Lastly, the project demonstrates the value of an integrated approach to program evaluation. The simultaneous lab and field measurements reinforce one another. For example, the carefully measured indoor airflows in the lab were useful for calibrating the field measurements of output capacity and the subsequent equipment efficiency. Further, the field data showed which operating conditions were important to investigate in the lab. Finally, both will be combined to produce energy modeling tools.

1. Introduction

The Northwest Energy Efficiency Alliance (NEEA) is a non-profit corporation supported by electric utilities, public benefits administrators, state governments, public interest groups, and energy efficiency industry representatives that operate in the states of Idaho, Montana, Oregon, and Washington. These entities work together to make affordable, energy-efficient products and services available in the marketplace.[1]

NEEA hired the team of Ecotope, Inc., supported by Research Into Action, Inc., Stellar Processes, and Herrick Labs, to evaluate the Northwest Ductless Heat Pump Pilot Project. The pilot project ran from October 2008 to December 2009. The DHP Pilot Project sought to displace zonal, electric resistance heating equipment, such as baseboards, with DHPs. The DHP Program, which succeeded the pilot project in 2010, continues to address this goal.

As an integral part of the Ductless Heat Pump Evaluation Project, Ecotope carried out an extensive laboratory analysis of DHP performance. The lab evaluation was designed to develop a detailed understanding of DHP performance for use in simulation tools and to support the field monitoring and subsequent data analysis of DHPs installed in homes. This report describes the equipment selected for detailed lab investigation, the methods used in the evaluation, the performance mapping results, and the performance model developed from the data for use in energy prediction tools. The work reported here will also be used to inform metering results from the field installations. That subsequent portion of the analysis will be included in a broader report after the field data has been collected and analyzed.

Like all heat pumps, single point ratings of performance are published following guidelines specified by the Department of Energy (DOE) and Air-Conditioning Heating and Refrigeration Institute (AHRI). The rating points, such as the heating seasonal performance factor (HSPF) and seasonal energy efficiency ratio (SEER), depend on a single curve describing the performance of the equipment over a temperature range which is essentially continuous and predictable. For conventional split system heat pumps the single rating point is marginal, at best, for determining energy use (Francisco 2004). Likewise, although the AHRI standard (AHRI 210/240-2008) has specific tests for variable speed equipment, early observations indicated that the ratings do not measure well the equipment response to changing control signals (Davis 2009). Moreover, existing field tests indicate DHP technologies often perform better than the ratings suggest by optimizing the outputs and inputs to the current environmental conditions (Geraghty, 2009). The efficiency and flexibility of the DHP systems stem from their ability to change thermal outputs and indoor fan flow in response to control signals from changing ambient conditions or the occupant. Therefore, a single rating point for variable speed DHPs can only represent a small fraction of the capable operational range. The lab testing and performance modeling of

[1] See the NEEA website at www.neea.org.

this project seeks to better understand DHP operation and energy use with an eye towards characterizing its savings energy saving potential.

1.1. Goals and Objectives

To support the project evaluation at large, the lab evaluation established the following goals:

- Develop a performance map of the equipment at all temperature bins and operating modes while providing special focus to low temperature heating performance.
- Assess performance variation with various control strategies and operating modes.
- Conduct measurements to review and verify the data collected in the field metering, especially *in situ* COP measurements.
- Establish empirical performance curves to predict the efficiency and output of the equipment in simulations (SEEM) or other engineering calculations. The modeling capability to be developed as part of this goal, in particular, will lead to directly supporting regional energy planning efforts and conservation program design.

To expand on the published rating values and to gather enough information for energy modeling, the lab evaluation was designed to measure the performance impacts on the equipment over the range of operating conditions that would be encountered in real installations. In practice, as the equipment is installed in climates that encounter both -5°F and +105°F temperatures, this creates the need for a performance map over a wide temperature range. The lab setting provides a stable, controlled situation to accurately and precisely measure equipment output as a function of environmental conditions.

Due to the continuously variable compressor design, the equipment capacity and efficiency is also variable. Generally, higher capacity output results in a lower system efficiency while the converse is true for lower capacity output. With this in mind, the lab performance mapping was designed to explore high, medium, and low capacities and also included high, medium, and low indoor fan speeds.

2. Methodology

Broadly, the test design called for steady-state measurements of efficiency with variations in outdoor temperature (and relative humidity), indoor temperature (and relative humidity), indoor fan speed, and compressor power. Additional tests with wet and dry indoor coils, outdoor frosting conditions, and equipment on/off cycling were also conducted. The methods and procedures used in the lab adhered to industry standards including ASHRAE Standard 116 and AHRI Standard 210/240. Appendix C includes a full definition of the test matrix applied to these two pieces of equipment.

2.1. Equipment Selection

The equipment to test was selected in conjunction with NEEA and other regional stakeholders. The priorities in selecting the equipment models included: frequency of occurrence of the specific model in the field, number of similar models installed in the field, range of HSPF/SEER ratings, age of model, and the number of field sites installed with the detailed instrumentation (in situ COP rig) package[2]. By selecting equipment that is frequently used in the field (or similar models) we will gain a better, direct understanding over that segment of houses. By covering a range of HSPF/SEER scenarios we can simulate a wider range of equipment. Next, by selecting newer, rather than older models, the lab data will be relevant farther into the future. The DHP equipment models are evolving and changing rapidly so selecting an older model might only represent many units installed in the early part of the pilot program while a newer model might represent 10,000s of units into the future.

Based on these criteria, we selected a Fujitsu 12RLS and Mitsubishi FE12NA. For the time period of the pilot project evaluation where the total number of units installed was 3,899, 7% of all units were the 12RLS. A total of 32% were Fujitsu units that behave in a very similar way[3] to the 12RLS. For the same period, 6% of installs used the FE12NA while we determined roughly 25% of all installations had comparable Mitsubishi units. Both units are recent models from the manufacturers representing the most mature equipment designs. The rated HSPF values were 12.0 for the 12RLS and 10.6 for the FE12NA. This range of performance is reasonably representative, if slightly skewed towards the high end, across most of the DHP installation in the pilot program. The trade-off for selecting equipment that will be relevant longer into the

[2] The field installed COP measurement package consists of supply and return air temperature sensors, airflow anemometers, and power meters. Using these measurements, the output capacity and input power are directly calculated.

[3] The definition of similarity between models was first constrained to units from a single manufacturer and then determined by observing behavioral trends from field monitored data. For example, some models exhibited a tendency to change compressor speed multiple times in an hour and "hunt" for an optimal setting regardless of the load, while others remained at stable speeds throughout that hour. Additionally, equipment from the same model line, differing only in rated capacity, was assumed to be similar.

future, was to evaluate models that perform above average in the current market. Table 1 shows the equipment specifications obtained from the manufacturers' literature. Throughout the report, the references to "manufacturer's literature," "spec sheet," and "published" data all refer to service manuals, design, and installation forms prepared by the manufacturers and obtain from their websites (Fujitsu 2009, Mitsubishi 2009).

Table 1. Equipment Specifications per Manufacturer's Literature

Model:		12RLS		FE12NA	
	Units	Rated*	Range†	Rated*	Range†
Cooling Capacity	Btu/hr	12,000	3,800-14,500	12,000	2,800-12,000
Heating Capacity	Btu/hr	16,000	3,100-24,000	13,600	3,000-21,000
Cooling Input Power	kW	0.83	0.20-1.53	0.93	0.16-0.96
Heating Input Power	kW	1.2	0.20-2.23	0.95	0.15-2.25
EER Cooling	Btu/hrW	14.46	--	12.9	--
COP Heating	kW/kW	3.9	--	4.2	--
SEER	Btu/hrW	25	--	23	--
HSPF (IV)	Btu/hrW	12	--	10.6	--
Power Factor Cooling	%	93	--		--
Power Factor Heating	%	95	--		--
Defrost		Reverse Cycle		Reverse Cycle	
Compressor Type		DC Inverter-driven Rotary		DC Inverter-driven Rotary	

* Rating conditions: 47°F outside temperature for heating. 95°F for cooling. Compressor operation at manufacturer determined intermediate speed. Indoor fan on high flow rate.

† Capacity and power range covers all outdoor temperatures and operating conditions – not just the range at the rating conditions.

The purpose of the report was not to select two heat pump models to directly compare, although some comparisons are inevitable. Instead, the intention was to pick equipment representative of DHPs installed in the field during the DHP Pilot Project and models offering a variety of control possibilities to better increase our understanding of DHP operation. The selected equipment is among the highest performing in the manufacturers' product lines, so the results can be more readily applied to future equipment even as this technology evolves.

2.2. Testing Facility

The performance mapping was conducted under contract to Herrick Labs within the Mechanical Engineering Department at Purdue University. Herrick Labs has tested and modeled the performance of vapor compression refrigeration cycle equipment for several decades. Ecotope has contracted with Herrick Labs since 2004 on a number of heat pump performance investigations. For the past projects and the current one, Ecotope acts to manage the lab work, which includes devising a test strategy, creating a matrix of testing conditions, providing guidance and quality control to the testing process, validating the data, and producing performance curves with the results. Herrick Labs carries out the test strategy by installing the necessary instrumentation, conducting the measurements, and reporting the results.

Figure 1. Herrick Labs Control and Data Logging Station for Psychrometric Chambers.

(The psychrometric rooms are entered through the doors to the left (simulating outdoor conditions) and right (simulating indoor conditions) of the computer terminals.)

The main equipment used in the testing are two, side-by-side ASHRAE standard psychrometric chambers (see Figure 1). Each chamber is an insulated room with independently controllable temperature and humidity using a computerized control system. The controllable temperature range of the rooms is from about -15°F to 125°F. For the testing, the outdoor unit of the DHP was installed in one chamber while the indoor unit was installed in the other (see Figure 2). Refrigerant and control lines are connected through ports between the chambers. The indoor unit is attached to a discharge plenum which is ducted to an ASHRAE standard air measurement box to observe air temperature and flow to determine the air-side capacity. The outdoor coil air flow rate is not measured directly but can be identified using an energy balance. A set of instrumentation is also installed on the refrigerant lines to measure mass flow, temperature, and pressure in order to calculate a refrigerant-side capacity. Throughout the performance mapping process, these capacities are compared. The good agreement between the two verifies the validity of the measurements.

Figure 2. Equipment Installed in Psychrometric Chambers.

(Outdoor unit instrumented at left: note grid of nine thermocouples monitoring outdoor air inlet temperature. Indoor unit at right: note window in green, insulated discharge plenum to allow remote controller to signal instructions to the equipment.)

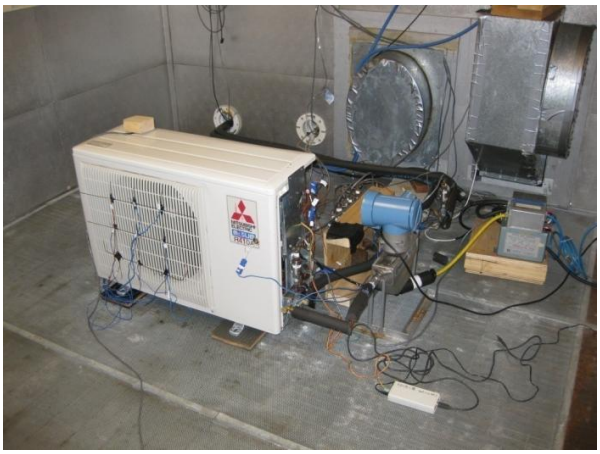

2.3. Instrumentation and Measurements

Each ductless heat pump under evaluation was instrumented to make the following measurements. The specific instruments used are described in Appendix B.

- Compressor input power
- Fan power for both the indoor and outdoor units
- Total heat pump power (including controls, fans, and compressor)
- Refrigerant flows, pressures, and temperatures: refrigerant flow is measured in the liquid line whereas pressures and temperatures are measured for the compressor suction line, compressor discharge line, liquid line, and inlet to the evaporator
- Indoor coil supply air temperature, humidity, and flow
- Indoor coil return air temperature, humidity, and flow
- Outdoor coil inlet and outlet air temperatures (humidity not recorded)

2.4. Indoor Unit Airflow and Output Capacity Measurements

A crucial measurement to all of the lab tests and, indeed, the field measurement sites with the COP rig, is the accurate determination of airflow across the indoor coil. Knowing the airflow is necessary to calculate the "air-side" output capacity of the equipment. The capacity is determined by using the measured temperature difference between the supply and return air of the indoor unit and the airflow rate. The lab computes both this "air-side" capacity as well as a "refrigerant-side" capacity which comes from measurements of refrigerant temperatures, pressures, and flows. The field measurements compute capacity based only on the air-side method so the lab data is used as a reference for field air measurements.

The lab measures the airflow by monitoring the pressure drop across a known orifice. The orifice is one of several nozzles inside a box set up in accordance with ASHRAE Std 41.2, Standard Methods for Laboratory Airflow Measurement. Measuring the flow requires ducting the ductless air discharge from the indoor unit to the nozzle box. Since adding a discharge plenum and duct system to the ductless unit creates additional static pressure for the indoor fan whereby reducing the airflow, the lab added a booster fan inline with the duct to match conditions that would exist for the indoor fan discharging into free air. To do so, the lab measured the fan power as well as the pressure drop across the indoor unit heat exchanger both before and after the discharge plenum was attached. The booster fan is then set to a flow level to match the indoor unit fan power to the values observed during the free air discharge case.

A central component of the lab testing approach was the simultaneous measurement of air-side and refrigerant side capacity. The measurements taken to determine each come from independent sensors. As stated previously, there is a set of temperature, pressure, and flow meters for the refrigerant and another for the air. Collecting data in this way is tantamount to performing two independent measurements to determine one quantity. If one measurement disagrees wildly from the other it could indicate a spurious data point. Further, if the one method consistently yields higher or lower values than the other, it could expose a bias in the measurements. Finally, when both consistently agree, it demonstrates a check on the experiment and verifies the results. Throughout the testing, both air and refrigerant side calculations are monitored for agreement to confirm the results.

2.5. Heating Mode Tests

In the Pacific Northwest climate, the cost-effectiveness of residential applications of DHP technology depends on the performance of the equipment during the heating season. As a result, the testing matrix and the analysis of these lab results have focused heavily on the efficiency of the DHPs in heating mode. Heating mode tests include steady-state, cycling, and defrost tests. The steady-state points are collected over the entire operating range of the equipment to form the basis of the equipment performance map. Cycling and defrost tests are special cases that impact the warm temperature and cold, humid temperature operation.

Steady-state testing conditions cover heating at outdoor temperatures from -5ºF to 65ºF at approximately 10ºF increments. For each set of ambient conditions, different combinations of fan speed and compressor speed ranging from minimum to maximum were used. For the list of specific data collection points (the test "suite" or test "matrix"), see Appendix C. In addition to the full performance map, all of the AHRI 210/240 tests specified to calculate the HSPF and SEER values were carried out.

The matrix was designed to optimize test time by testing a combination of compressor and fan speeds at the high and low temperature extremes and then filling in between with a smaller set of likely fan and compressor speeds. One goal was to include extreme points for both temperature and compressor speed in an attempt to cover the vast majority of operating conditions. The valid range of any performance model will be limited by the extreme test points beyond which any values must be extrapolated with less certainty. For operating conditions within the testing range, the performance values can be interpolated between measured data points thus increasing certainty.

The majority of tests were conducted at a single indoor ambient air temperature of 70°F. A subset was conducted at varied indoor temperatures (60°F, 65°F, and 75°F) to observe the effect on indoor coil performance. The results show a predictable dependence on indoor temperature that also agrees with the available manufacturer's data. Broadly, cooler indoor temperatures improve efficiency because they provide a colder temperature sink into which heat is rejected. The converse is true for higher temperatures. The indoor temperature dependence is important to measure because field work at DHP sites has shown rooms to be stratified. For the wall mounted units, the return air temperature will therefore be higher than the set point and general living space temperature which slightly decreases performance.

To collect the steady-state data, the operating parameters are set and the equipment is run until it reaches a stable state. The stable state is defined as being reached when no monotonic changes in refrigerant discharge temperature are observed over a 10 minute period. Data is then logged over the next 10 minute interval and averaged to a single value for each measurement point. The refrigerant discharge temperature is a good indicator of system state because it is influenced by both compressor speed and the electronic expansion valve (EEV) position. The equipment typically adjusts its compressor speed very quickly (approximately 30-120 seconds) to respond to load changes and then optimizes operation by slowly[4] adjusting the EEV to meter refrigerant flow.

Different strategies were employed to get the compressor to operate at the desired output. For the FE12NA, Mitsubishi provided a controller which uploads a program to the unit's logic board and forces it into a certain compressor and fan speed combination. This covered some, but not all of the desired mapping points. For the 12RLS, there was no controller available for the testing. In those cases, a combination of fixing the psychrometric chamber's temperature and the DHP's set point was used to drive the compressor operation. For example, by setting the DHP set point 6 ºF above the room temperature, the DHP runs at high output. Conversely, by setting the DHP to a set point close to the room temperature, the DHP runs at minimum output. Intermediate compressor loadings were more challenging to obtain since the lab had to experiment with what temperature set point combinations would produce a mid range compressor power draw and stable operation. Fan speed is easily set and fixed via the standard remote control.

Neither the unit itself nor the equipment controller displays the compressor operating speed (frequency). Both Ecotope and the lab considered different approaches to directly measuring the rotational frequency including the use of an accelerometer mounted to the compressor in the outdoor unit but ultimately opted against this measurement due to time constraints. Instead, throughout the project and this report, we assert that the compressor power measurement is a

[4] The speed of EEV adjustment varies by equipment model. The major adjustments happen in conjunction with the large changes in compressor speed while minor adjustments can continue for many 10s of minutes longer. For example, in many instances, the FE12NA was observed to take 2 hours to reach a stable state. In contrast, the 12RLS often stabilized in a quarter to half the time or sooner. Note: these are rough approximations.

surrogate for speed. From an energy performance modeling perspective, knowing the speed is not necessary but input power and output capacity are. Therefore, the performance mapping goals of the project were not compromised by not having this measurement. The standard equipment ratings are based on compressor frequency (see Section 6) but with no direct way to set the frequency, not being able to measure it did not prove to be a disadvantage. Measuring and documenting the relationship between frequency and input power may provide further insight into how the equipment operates. Therefore, future projects may want to consider a direct measure of speed but the successful completion of the performance maps and subsequent modeling (see Section 7) for this project show it was not necessary.

2.6. Cooling Mode Tests

The procedures for the steady-state cooling tests are similar to those outlined for heating: for each operating condition, different combinations of fan speed and compressor speed are used ranging from minimum to maximum speed. As in heating mode, different combinations of indoor air conditions were explored. Unlike heating, cooling performance depends on the indoor air moisture content, not just the temperature. The moisture content of the indoor air, and the indoor coil state, either wet or dry, affects the sensible, latent, and total cooling capacities. Therefore the performance map included variations in indoor relative humidity and the lab also monitored the split between sensible (temperature change) and latent (dehumidification) cooling capacity.

The main indoor air conditions were 80°F dry bulb, 67°F wet bulb which are the most common conditions for the EER and SEER tests. Additional tests included 80°F db with variations of 58°F, 62°F, 65°F, and 72°F wb as well as dry coil tests with 70°F, 80°F, and 85°F db. For the complete cooling mode test matrix see Appendix C. The cooling mode matrix shows that different numbers of tests were conducted on the FE12NA and the 12RLS. The larger number of the FE12NA was done when the lab realized more tests were needed to characterize the performance variation.

3. Airflow and Capacity Measurement Comparison Results

3.1. Indoor Unit Airflow Measurements

The airflow measurement results for both equipment models are given in Table 2 and Table 3. For comparison, the literature values from the technical and service manuals for the units are also shown. Both tables show the high efficiency levels of the indoor fan. The 12RLS ranges from 0.05 W/CFM to 0.8 W/CFM. The FE12NA ranges from 0.04 W/CFM to 0.07 W/CFM. One reason the fan power remains so low is that both models are pulling return air from and discharging supply air to free space with little resistance to flow. Regardless, both draw little power across the range of flows.

Table 2. 12RLS Indoor Unit Airflow Measurements

Fan Setting	Measured Values				Literature Values *
	Heating		Cooling		Heating and Cooling
	Flow (CFM)	Power (W)	Flow (CFM)	Power (W)	Flow (CFM)
Low	251	12	286	14	274
Med	348	21	378	25	374
High	425	29	487	39	453

* from Fujitsu Design and Technical Data for 12RLS

Table 3. FE12NA Indoor Unit Airflow Measurements

Fan Setting	Measured Values				Literature Values *	
	Heating		Cooling (wet)		Heating	Cool (wet)
	Flow (CFM)	Power (W)	Flow (CFM)	Power (W)	Flow (CFM)	Flow (CFM)
Low	149	6	144	5	166	144
Med	217	10	204	8	240	202
High	337	24	338	23	399	350

* From Mitsubishi Service Manual for MSZ-FE12NA

3.2. Air and Refrigerant Capacity Measurement Comparison

The comparison results of the air-side and refrigerant-side capacity measurements for the steady state tests are depicted in Figure 3, Figure 4, and Figure 5. In the figures, the closer the ratio of the air-side to refrigerant-side capacity is to one, the closer it appears to the 45° line showing concurrence. For some of the cooling tests, the refrigerant entering the flow meter or exiting the evaporator was in both the liquid and gas phase so its mass flow rate could not be metered. Therefore, no refrigerant-side capacity was calculated. All of the FE12NA cooling tests exhibited two-phase flow so no comparison data is available. Approximately half of the steady state cooling tests for the 12RLS showed two-phase flow. The ones that did not are compared in the plots. Overall, for the heating and cooling calculations available, the air-side and refrigerant-side measurements showed agreement to within ±6% of one another in the steady state tests. Because of the close agreement, the air-side calculations can be relied upon to determine

capacity for the cases where the refrigerant measurements could not be made. Finally, the agreement between the two measurement methods demonstrates the veracity of the determination of output capacity.

Figure 3. Capacity Measurement Comparison for 12RLS Data.

(Data points in blue. Red dashed line is the 45° line showing agreement.)

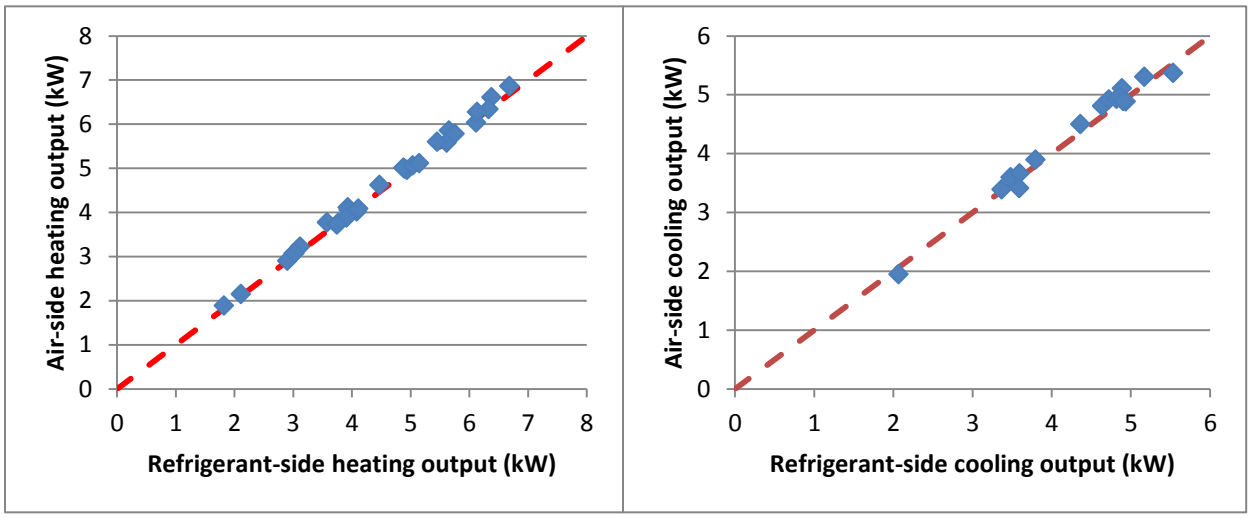

Figure 4. Capacity Measurement Comparison for FE12NA Heating Data.

(Data points in blue. Red dashed line is the 45° line showing agreement.
Cooling data comparison not available.)

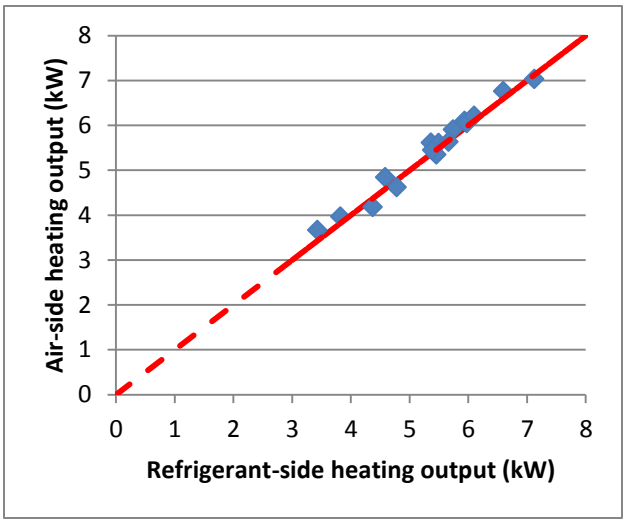

4. Heating Performance Map Test Results

When looking at the full results from the steady-state tests, the fully variable speed nature of the equipment becomes apparent. The variety of compressor and fan speeds combine to offer a huge range of input powers and output capacities to meet the space conditioning load. A clear trend from the data shows that the higher the output capacity, the lower the efficiency. Equipment performance is maximized when the loads are small. This is true for both heating and cooling. Additionally, the ability of the equipment to run at a very low speed will greatly reduce the amount of time the equipment must cycle on and off in low load situations. This on-off cycling is a performance penalty for single speed heat pump systems but, in comparison, is largely avoided with the DHP variable speed equipment.

The main variables determining the system capacity are outdoor temperature and humidity, indoor temperature and humidity, indoor fan airflow, and total input power. In single speed systems, indoor airflow and compressor frequency are fixed but the inverter-driven DHPs can change these according to demand adding two more variable aspects to the capacity. When plotted together, the large set of variables creates a complex space of data points. To simplify the plots and isolate certain effects, the plots in this report show only variation among a select few of the inputs on a given graph.

4.1. Steady State Heating Capacity and Input Power

Figure 5 and Figure 6 show the heating capacity of the 12RLS and FE12NA for 70°F indoor temperature[5]. High compressor speed tests are plotted in blue, medium in red, and low in green. Figures D1 and D2 in Appendix D are similar plots but show steady state input power as a function of capacity. In practice, the later set of figures is more closely aligned with how the equipment controllers work but is a less traditional way of graphing heat pump data. Given a desired set point, as set by a remote control thermostat, the DHP will change its input power to attempt to meet the load. This is discussed further in the performance model section. The available literature data on capacity and input power are plotted in the Figure 5 and Figure 6 for comparison to the lab measurements. The manufacturer selected data lies in the middle of the operating range and generally includes the nominal rating point[6].

The heating capacity and input power of the two models should not be directly compared because they are rated at slightly different sizes. The 12RLS has a nominal output rating of 16,000 Btu/hr at 47°F while the FE12NA has a nominal output rating of 13,600 Btu/hr. As

[5] Additional data were collected at indoor temperatures different from 70°F temperature but are not shown here. When the indoor temperature is higher, system capacity and efficiency decreases slightly. The converse is true for lower indoor temperatures. The data were used in developing the performance model.

[6] The nominal rating point refers to the conditions under which the rated capacity is measured. For heating, this is output at 47°F outdoor, 70°F indoor, and intermediate compressor speed. For cooling, it is 95°F outdoor, 80°F at 50% RH indoor, and intermediate compressor speed.

Figure 5 and Figure 6 indicate, this nominal rating is squarely in the middle of the output range. This is typical of all DHP equipment labeling. One reason is the equipment often operates in the middle of the load range. In fact, the equipment controls appear to differentially choose to operate at this set of speeds suggesting that such a choice might be the most accurate estimate of overall performance.[7] Another potential motivation is that, by listing a nominal output in the middle of the compressor range, the performance rating will be higher than that of a maximum output capacity.

Figure 5. 12RLS Steady-State Heating Capacity for Indoor Temperature of 70°F.

(Equipment input power and indoor unit fan speed are shown below each point. The measured outdoor coil inlet temperatures were unavailable so the temperature for the outdoor psychrometric chamber is used in the plot.)

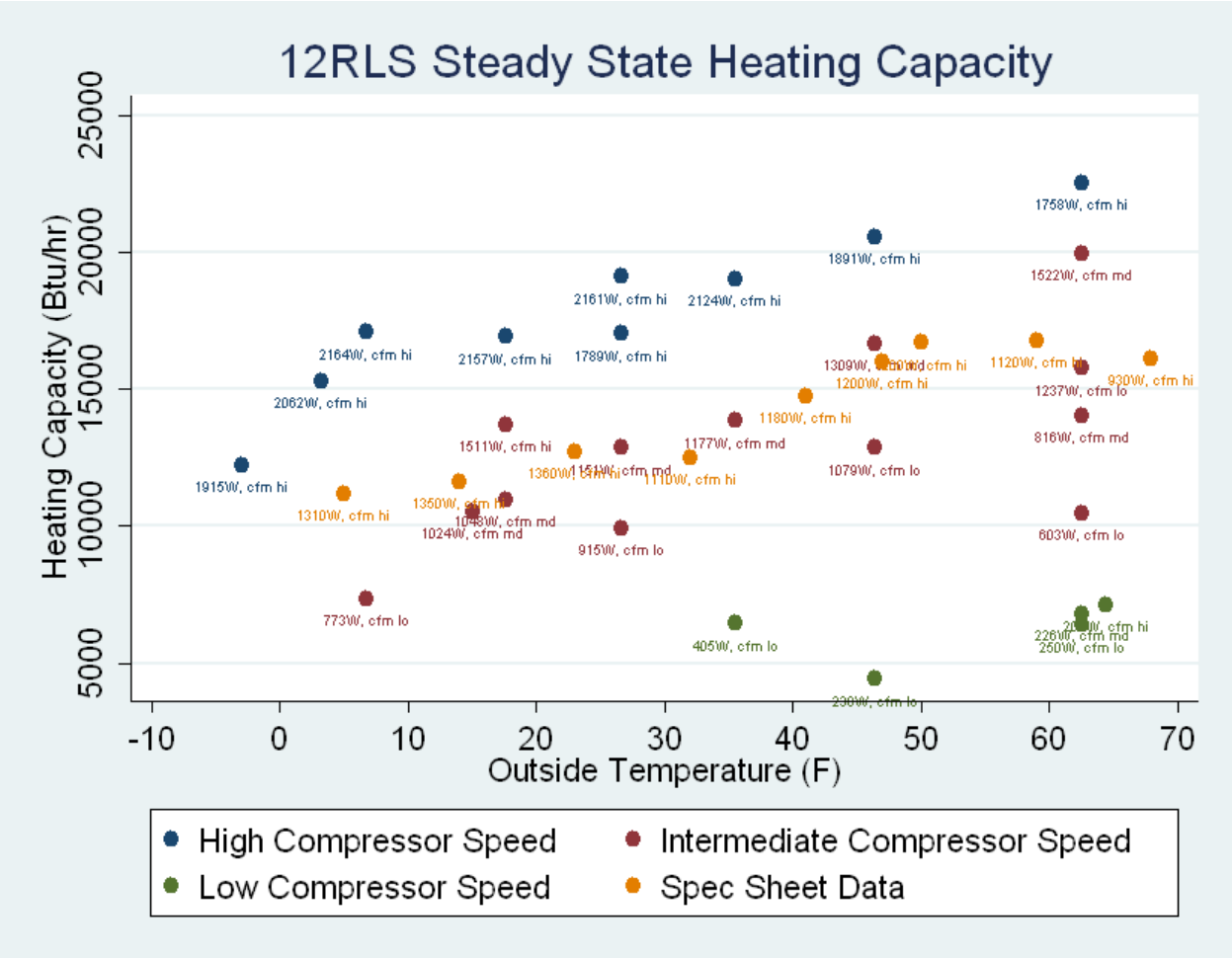

[7] Field data in particular, shows again and again, the preponderance of equipment operation in mid-capacity ranges.

Figure 6. FE12NA Steady-State Heating Capacity for Indoor Temperature of 70°F.

(Equipment input power and indoor unit fan speed are shown below each point. The measured outdoor coil inlet temperatures are used in the plot, which differ slightly from the targeted set point of the psychrometric chamber.)

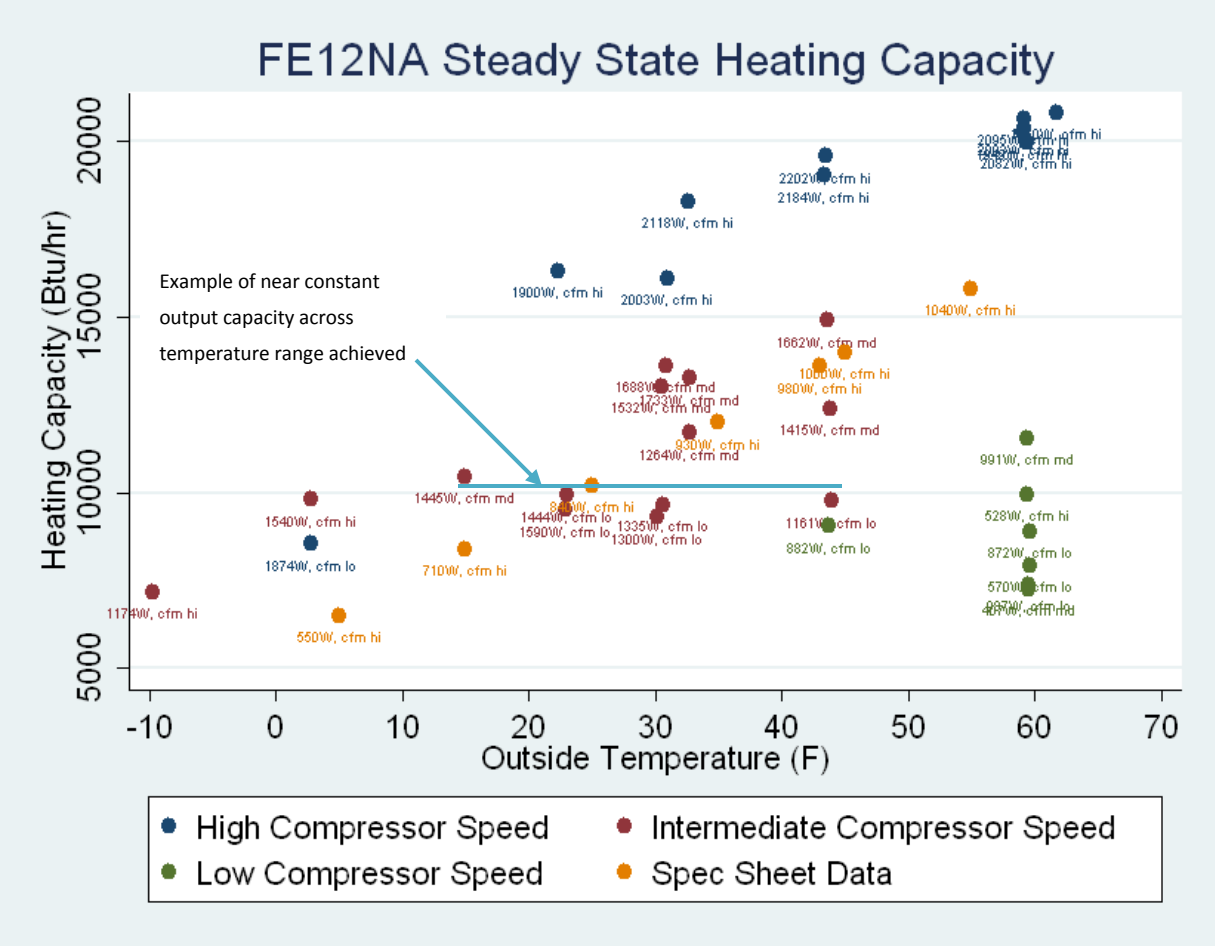

Both Figure 5and Figure 6 show the expected trend of decreasing output capacity with decreasing outdoor temperature. The trend is somewhat obscured by the fact that the equipment has variable input power but it is clear for the maximum compressor speed (blue points with highest capacity) which, to a first approximation, has a fixed input power. The blue plots always reference tests that targeted the maximum compressor speed. Some of these tests stabilized at less than maximum capacity. In those cases, the data was recorded, classified in the high capacity range, and the test restarted. Other max speed tests were paired with lower indoor fan flow rates which results in lower capacities. Next, the figures also demonstrate the effect of hypothetically fixing the output capacity. For instance, Figure 6 shows that the FE12NA outputs about 10,000 Btu/hr at 15°F using 1400W whereas a similar output is achieved at 45°F using 1100W.

Figure 5, in particular, shows low equipment input powers at low load conditions. There is a cluster of data points from 50-60°F with power draws of 225-300W which indicates light loadings and low compressor speeds. That the DHP could operate at such a low partial load was an unexpected finding. Conditions for heat transfer are obviously favorable at such warm

outdoor temperatures but the DHP also exhibits the ability to operate at a low part load at even lower temperatures (~40°F).

4.1.1. Steady State Heating Efficiency and Field Agreement

The steady state heating coefficient of performance (COP) is shown in

Figure 7 and Figure 8. COP is defined as output capacity divided by input power. Both plots demonstrate the high efficiencies possible from DHPs. They also show the range of COP due to variations in compressor load: a lower load always leads to a higher efficiency. In the plots, as with Figure 5and Figure 6, low load points are green, medium load are red, and high load are blue. As with earlier plots, the literature data is also shown in yellow. In addition to the lab results, the figures plot data obtained from field-monitored COP sites (light gray box plots)[8]. The results suggest a consistent relationship between outdoor temperature and COP. While the result is expected, there is also clear agreement between both the field measurements and the controlled setting laboratory measurements. The ability of the observed data to follow the curves derived from the lab (in spite of variations in compressor speeds as the equipment meets the loads of the house, defrost behavior and occupant intervention) provides confidence in using the lab data to develop performance prediction models.

Both

Figure 7 and Figure 8 show strikingly high levels of performance at low temperatures. For temperatures from -10°F to 10°F, the steady state COPs are still shown to be 1.5 to almost 2.5. Actual performance is less because the equipment undergoes defrost cycles which are, by definition, not in steady state. The box plots from the field data are more representative of actual performance because they include both defrost events at low temperatures and cycling effects at warmer temperatures.

The range of efficiencies for a given temperature can be seen in

Figure 7. For example, tests of varying compressor and fan speed at 47°F show a COP of 3.2 at maximum load to a COP of greater than 5.5 at a low load.

Figure 8 demonstrates agreement between the lab results and the field measurements. The published performance curve, however, differs especially at low ambient temperatures from the other two measurement sources. This could be partly explained by defrost behavior. Additionally, some of the variation is clearly due to the selected published data being at low load for the low temperature range. For instance, the 15°F and 25°F data points are only at 58% and 75% of nominal input power respectively. In contrast, operation in an actual house at these

[8] The field data includes six sites for each equipment type and spans a full range of winter temperatures. The box plots represent the upper and lower quartiles, the median value is given as the band in the middle, the upper and lower whiskers are the maximum and minimum observations.

temperatures is likely to require far greater input and output to meet the heating load[9]. These higher loads will reduce the COP. Lastly, the variation could be due to other factors in the test procedure which are discussed in subsequent sections.

Figure 7. 12RLS COP Plot.

(Field data given as box plots. Steady state lab data plotted as points.)

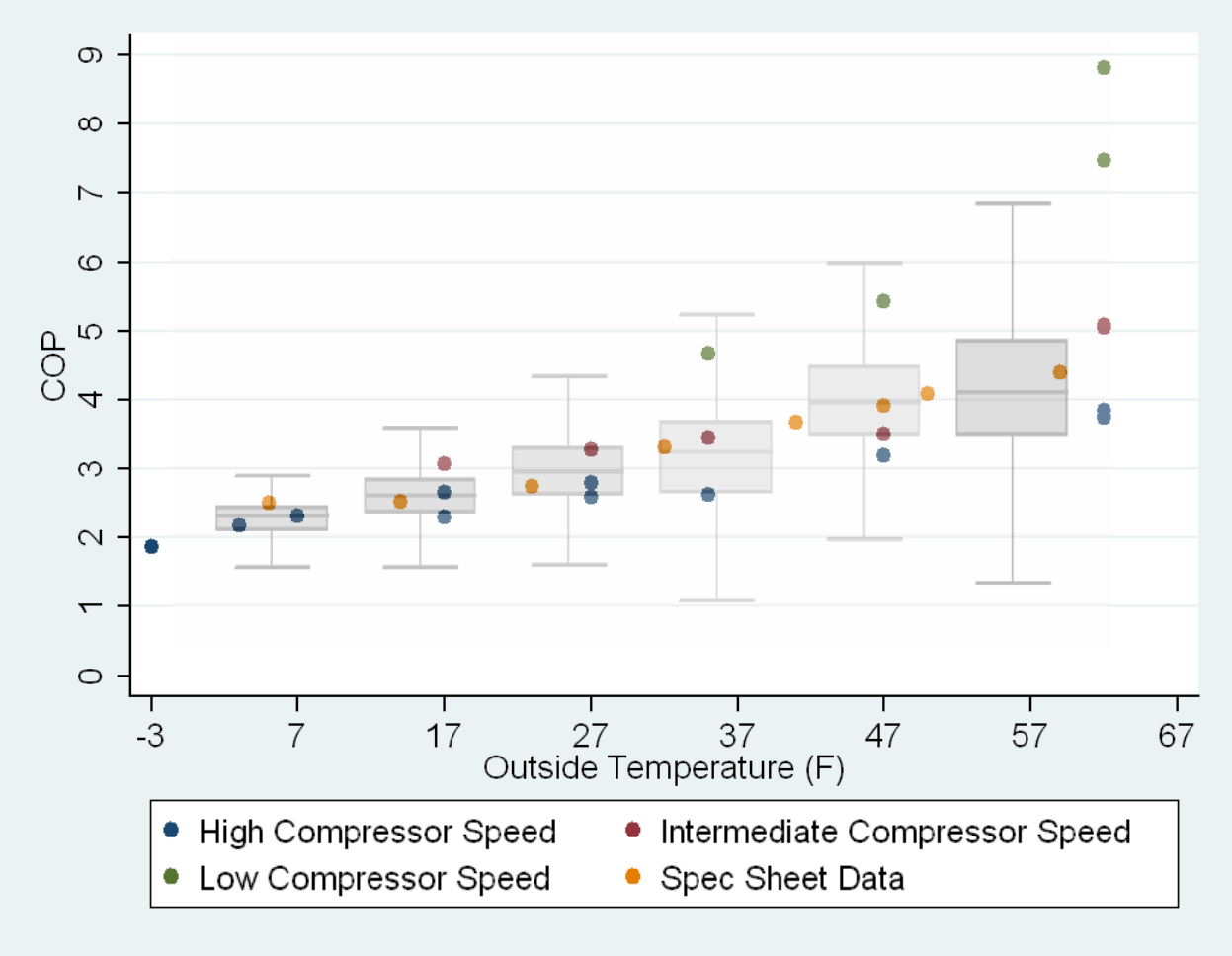

[9] Field data confirm this.

Figure 8. FE12NA COP Plot.

(Field data given as box plots. Steady state lab data plotted as points.)

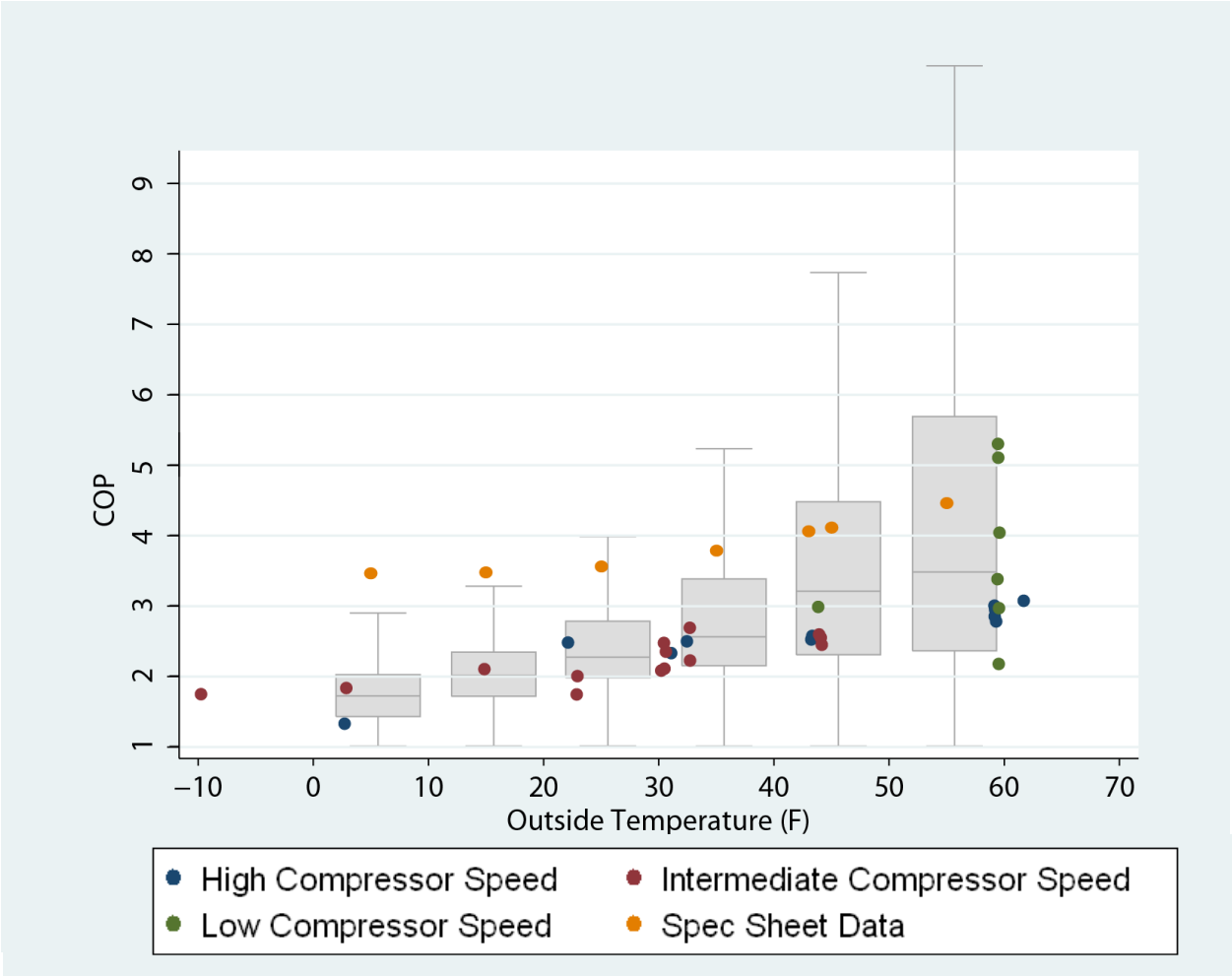

4.2. Defrost Cycle

In heating mode, the DHP outdoor unit acts as an evaporator which extracts heat from the outdoor air. In the process, the outdoor coil cools down considerably creating a condensation and nucleation site for ambient water vapor. The subsequent build-up of frost leads to increasingly poor heat transfer from the air to the refrigerant. To address this problem, the DHP will periodically initiate a defrost cycle which reverses the hot refrigerant vapor flow to melt the ice. The two equipment models considered here (and, indeed, all of the observed models in the pilot program field study) use a reverse cycle defrost method.

The DHP monitors outdoor temperature, run time, and refrigerant pressures to identify trends associated with frost formation. The precise strategy to determine the time to initiate a defrost cycle varies with equipment model. When the cycle initiates, the controller turns the compressor and the indoor fan off. Typically, the DHP also illuminates a light on the indoor unit indicating defrost operation to the occupant. Next, the controller switches the direction of the 4-way valve to reverse refrigerant flow. The compressor is subsequently turned on again so now the outdoor coil is acting as a condenser. Then, the compressor runs (with the indoor fan off), adding heat to the refrigerant, which melts ice off the coil. After the ice melts, the controller returns the DHP to normal heating operation. Alternatively, the defrost time may exceed a default limit set by the controller and the equipment returns to heating mode before satisfying all of its defrost criteria and potentially not melting all the ice. Since the DHP, without integrated auxiliary resistance heat, provides no heat to the space during defrost, the maximum defrost time is designed to limit the amount of time without heating regardless of coil conditions.

Figure 9 plots the data from the 12RLS 35°F defrost test. Per the AHRI 210/240 procedure, the equipment is observed through two defrost cycles. Data used to calculate the defrost penalty is taken from the second cycle. The defrost penalty is the amount of energy used in the cycle that does not go towards heating the space. Figure 9 shows two full cycles with quasi-steady state operation before each defrost event (which start at minutes 90 and 220). Before defrost occurs, the green COP plot shows a noticeable decline in equipment performance. The yellow plot of refrigerant temperature at the evaporator outlet serves as a proxy for frost accumulation on the coil. Starting about halfway through each heating cycle, the evaporator outlet temperature begins to decline more rapidly indicating frost buildup. COP also drops off. For the defrost event, the compressor runs at about 650W. After defrosting, the COP increases as the equipment ramps up to meet the load and optimizes its EEV position and compressor speed.

Figure 9. 12RLS Defrost Cycles at 35°F.

(Data sampled at 10 second intervals.)

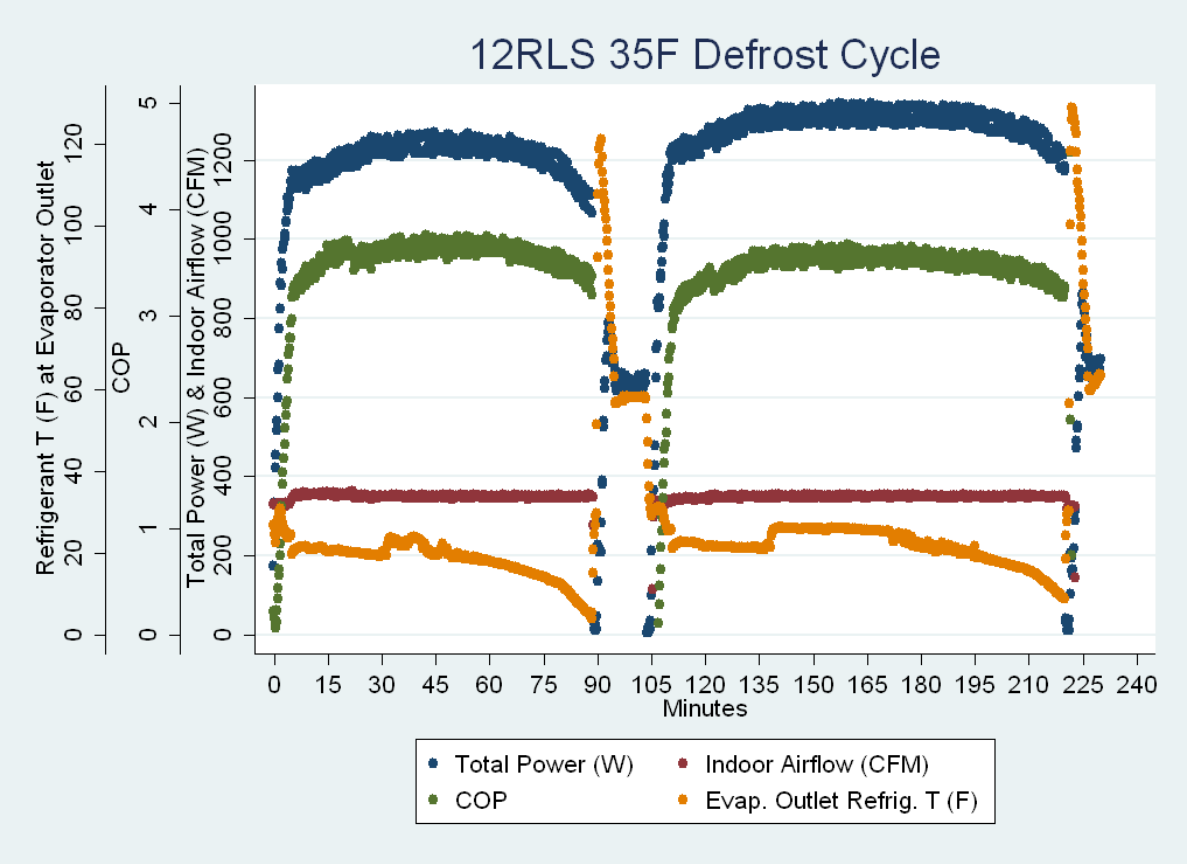

Our testing plan expanded slightly on the standard AHRI 210/240 defrost testing conditions to explore frosting at 47°F and 75% RH as well as at 35°F and 17°F. There are a significant number of morning hours with temperatures in the 40-50°F range and high relative humidity in the Northwest marine climate which can present frosting challenges to heat pumps. Neither the 12RLS nor the FE12NA showed frost buildup at the 47°F test point. Accordingly, no data were collected.

In testing the FE12NA, some unexpected opportunities arose to collect defrost data when the unit began frosting during the steady-state testing sequence. These data were added to the results and provide a more complete picture of defrost with the FE12NA. Table 4 shows the defrost test results in terms of equipment COP over the entire cycle. The table shows that defrost cycles occur more frequently and last a longer portion of the cycle at colder temperatures. Although the humidity ratio in colder air is less than warmer air suggesting the need for less frequent defrost, lab photos (see Figure 10) showed frost accumulated on the coil at even the -3°F (n3) test condition. Further, the whole cycle extends longer because the colder temperatures require a longer defrost time to warm up the coil.

Table 4. Defrost Test Results.

	Test code	Cycle Time (hrs)	Heating Time in Cycle (hrs)	Defrost Time in Cycle (hrs)	Fraction of Cycle Time in Defrost	Full Cycle COP	Heating-Only Segment of Cycle COP	Relative COP Penalty
FE12NA	H-SS-n3-H-MX	0.79	0.62	0.17	22%	1.35	1.52	11%
	H-SS-7-H-MX	0.52	0.48	0.04	7%	1.54	1.60	4%
	H-SS-7-L-MX	0.39	0.35	0.04	11%	1.08	1.13	5%
	H-SS-17-H-MX	1.51	1.45	0.06	4%	2.24	2.28	2%
	H-SS-17-M-MX	1.50	1.45	0.06	4%	0.88	0.89	1%
	H-SS-27-H-MX	1.31	1.28	0.03	3%	1.72	1.74	1%
	H-DF-35-M-MX	1.50	1.45	0.06	4%	1.76	1.78	1%
12RLS	H-DF-17-M-MX	2.35	2.10	0.25	11%	2.91	3.06	5%
	H-DF-35-M-MX	2.12	1.94	0.18	8%	3.29	3.39	3%

Test Code: H is heating, SS/DF for intended steady-state or defrost test,
-3/7/17/27/35 Outdoor T (F), H/M/L is High/Medium/Low fan, MX is Max compressor speed

Figure 10. Frost Accumulation on Outdoor Coil of FE12NA at -3°F.

(Moments before the defrost cycle is initiated)

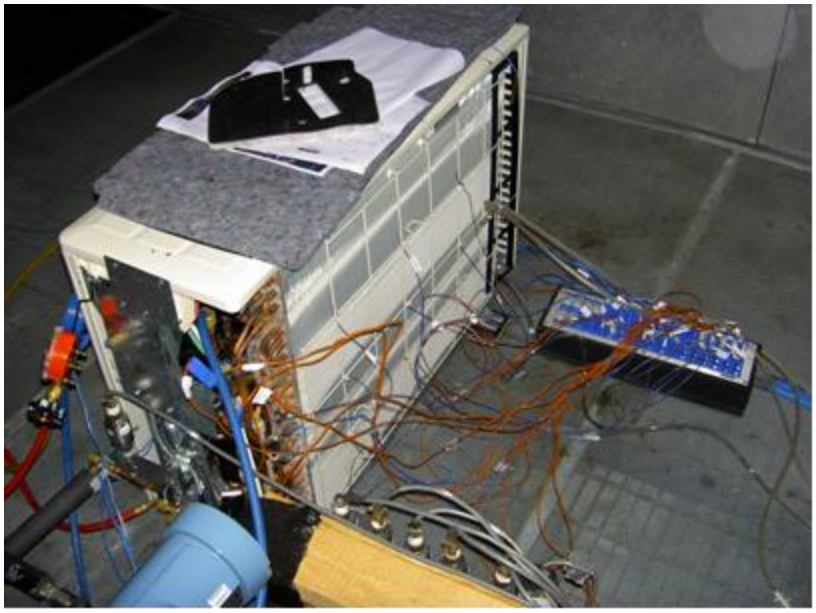

4.3. Heating Mode Cycling

Single speed heat pumps cycle on and off in order not to exceed the heating set point temperature. Only at peak load times do single speed systems run continuously. In contrast, variable speed DHPs turn down their input power in the response to a decreasing load and run continuously. Even so, there comes a point when the load required is so low, that the unit begins to cycle. In heating, this corresponds with warm outside temperatures. Therefore the standard heating cyclic mode tests are conducted at a 62°F outdoor temperature. Cycling comes at an energy cost associated with starting and stopping the system. The low load cycling tests capture this impact.

The heat mode cyclic degradation coefficient, Cd, as determined by the AHRI 210/240 standard was found to be:

- 12RLS C_d (heating): 0.28
- FE12NA C_d (heating): 0.45

In the context of single-speed heat pumps, both of these values for Cd are surprisingly high where we might see a Cd range from 0.05-0.15. For variable speed systems, Cd has a far less importance, however, since compressor can run at small load fractions instead of cycling. If the testing outcome results in a value greater than 0.25, the 210/240 standard calls for a replacement of the high value with 0.25 for HSPF calculation purposes.

When both the 12RLS and the FE12NA cycle on, their compressors initially overshoot the desired minimum load. After this initial spike, the compressors ramp down into the low load state. The higher power draw at the beginning of a cycle results in a performance penalty explained by Cd. The lab data shows the FE12NA ramps its compressor up higher than the 12RLS at the initial startup stages, which is why it has a larger Cd.

In order to use the cycling coefficient, it is necessary to know under what conditions the unit cycles. First, while it is the low load that causes the cycling, the practical limitation for the DHP is the minimum input power level needed for operation. The lab data shows the 12RLS will turn down to 220W and the FE12NA to 450W. This corresponds to roughly 20% of the rated and 10% of the maximum power for the 12RLS; and 45% of the rated and 20% of the maximum power for the FE12NA. This turn down fraction agrees with the specified data from Table 1 for the 12RLS but is about double for the FE12NA. Logged power measurements from field data support this finding.

4.4. Comparative Heating Mode Performance

It is somewhat challenging to directly compare the heating mode performance of the two variable speed DHPs because they have different responses across their load range. One can compare the performance at maximum capacity which will be especially relevant at low temperatures but could be misleading at higher temperatures where the control algorithms might use different strategies and speeds to meet the heating load. Figure 11 and Figure 12 show curve fits for the maximum heating capacity and COP at that capacity for steady-state data. The characteristics are similar between the equipment models at middle temperature ranges but diverge at both low and high temperatures. On an annual basis, high temperature maximum output is not critically important to energy use, but low temperature maximum and middle temperature intermediate

output are. The differences in maximum-capacity, low-temperature efficiency explain some of the performance variation in the two models. Since Figure 11 and Figure 12 show little variation in performance at maximum output over the mid-range temperatures, we can assert that most of the variation in performance occurs under the part-load conditions.

Figure 11. Comparative Input and Output at Maximum Capacity

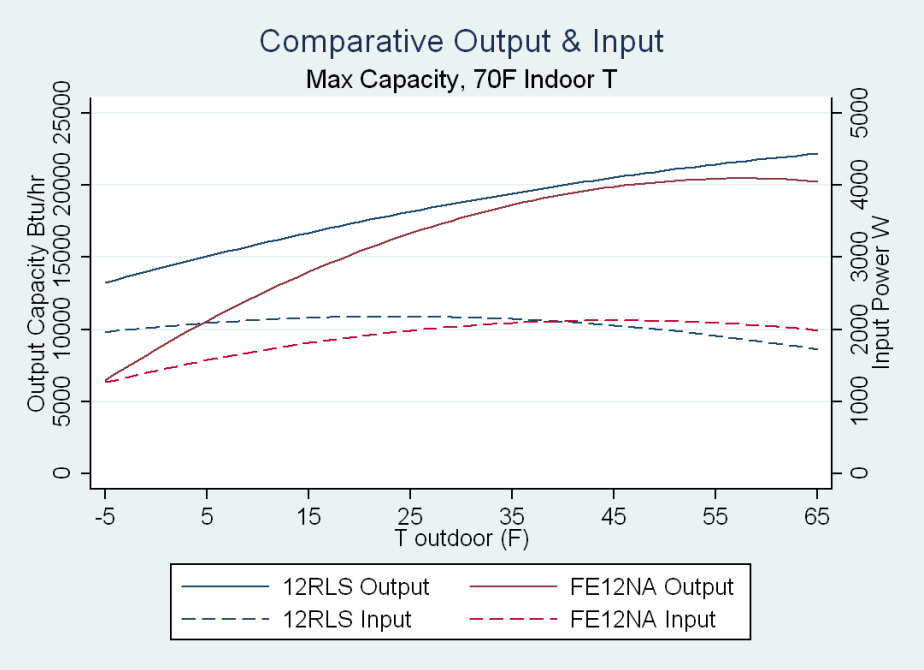

Figure 12. Comparative Efficiency and Maximum Capacity

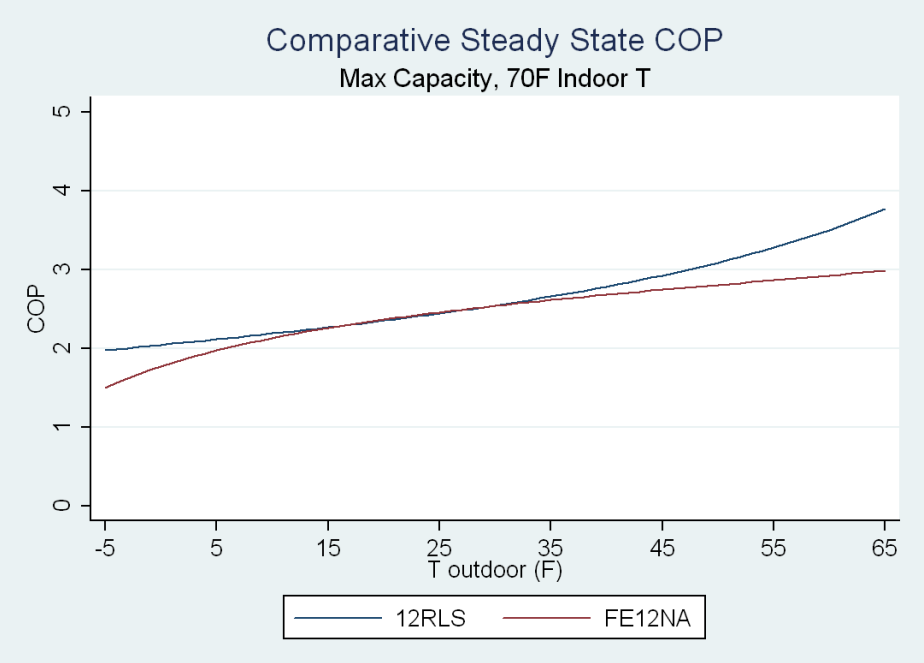

5. Cooling Results

The cooling mode tests were carried out in the same way as the heating mode. One difference in the results is the added dependence of performance on both indoor temperature and RH and the impact on sensible and latent cooling capacity. Further, outdoor coil frosting is not an issue in cooling so there are no defrost tests. In this section the illustrations are made at indoor conditions of 80°F and 50% RH. These are standard conditions used in calculating SEER. As of this writing, the cooling data from the field test is not available for comparison to the laboratory COP data.

5.1. Steady-State Cooling Capacity and Input Power

Figure 13 and Figure 14 show the cooling capacity of the 12RLS and FE12NA for 80°F (67°F wb) indoor temperature. For comparison, in addition to the lab measurements, the available literature data on capacity and input power are plotted in the figures. The manufacturer selected data lies in the middle of the operating range for the 12RLS but covers the higher end for the FE12NA. Both models are nominally rated at 95°F to deliver 12,000 Btu/hr of cooling. The corresponding input power requirements are 0.83kW for the 12RLS and 0.93kW for the FE12NA. In contrast to the nominal heating capacity of the FE12NA, which was in the center of the output range, the cooling nominal capacity is at the high end of the output range. The nominal output of the 12RLS in cooling is, like heating, in the center of the range.

Figure 13. 12RLS Steady-State Cooling Capacity for 80°F (67°F wb) Indoor Temperature.

(Equipment input power and indoor unit fan speed are shown below each point.)

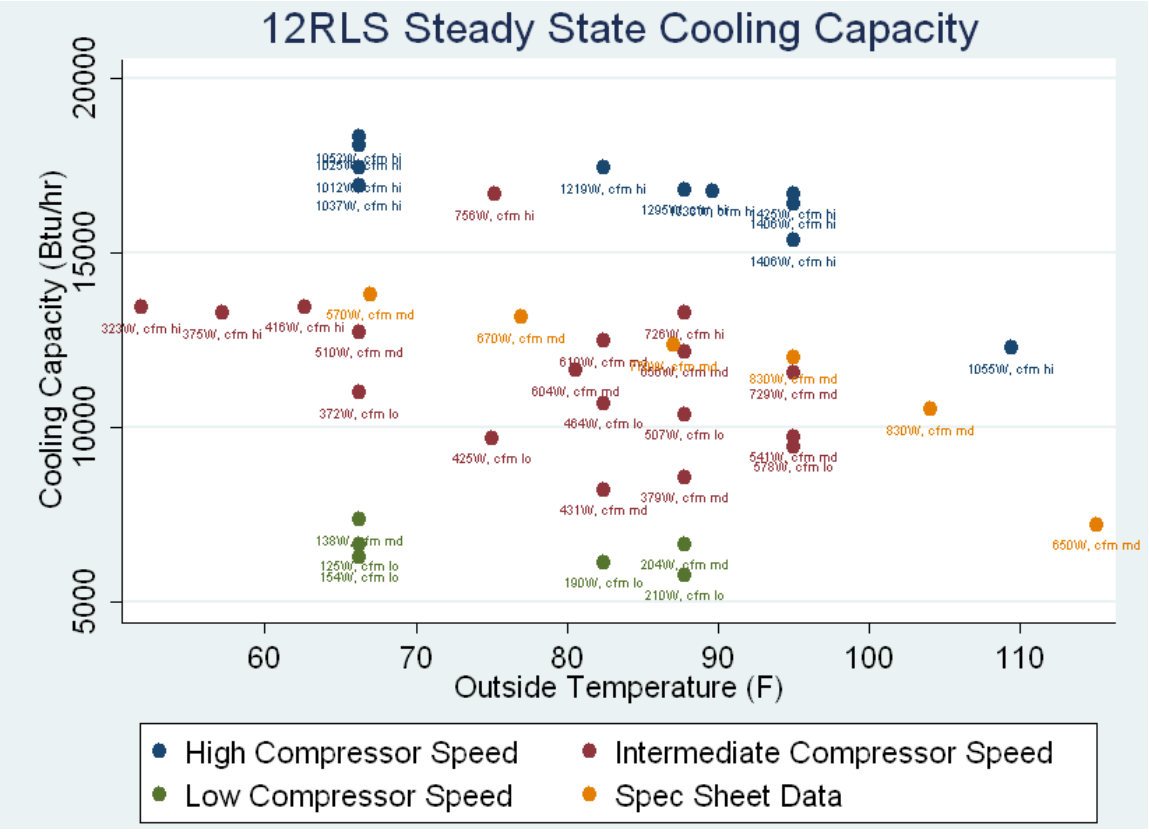

Figure 14. FE12NA Steady-State Cooling Capacity for 80°F (67°F wb) Indoor Temperature.

(Equipment input power and indoor unit fan speed are shown below each point.)

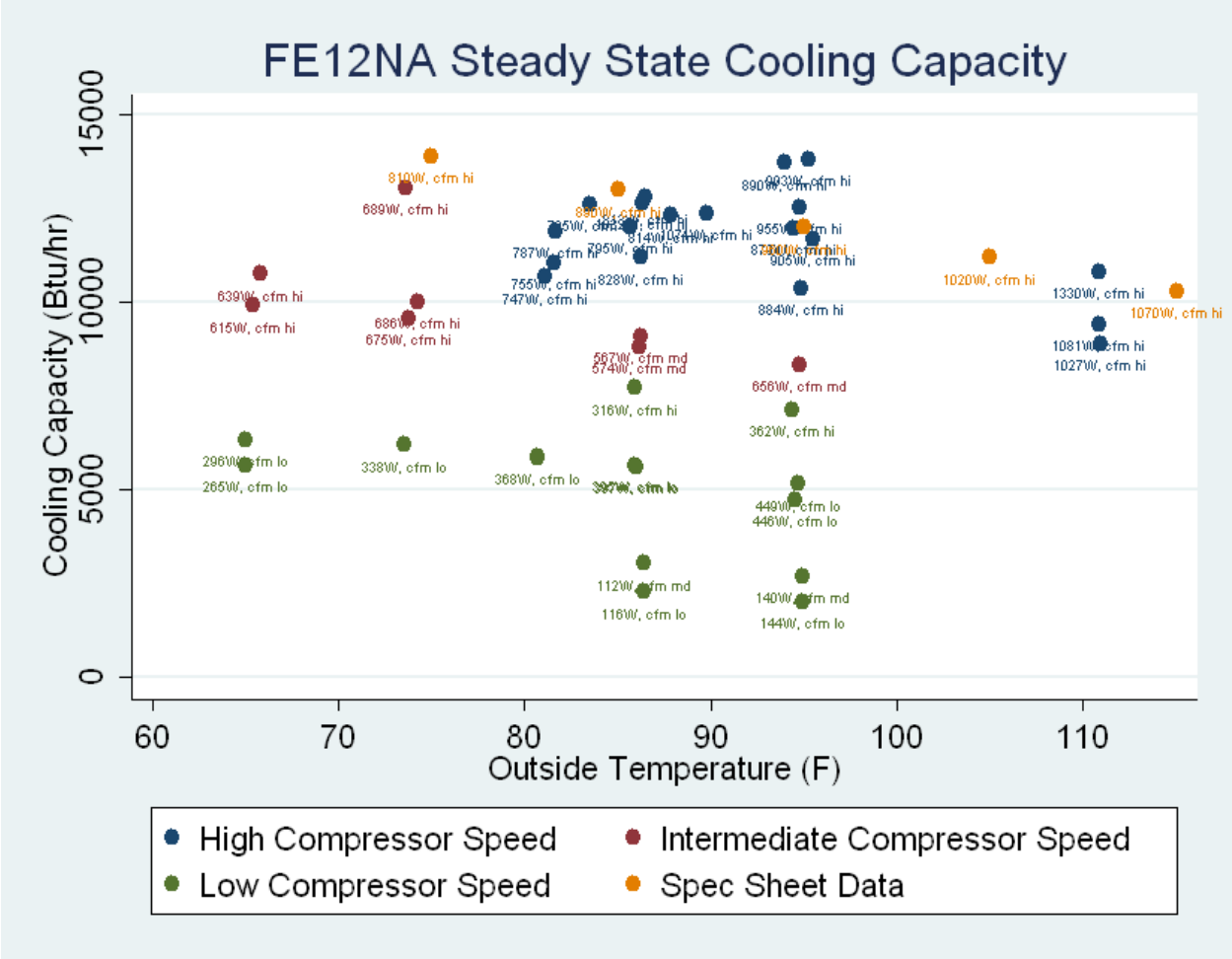

5.1.1. Steady State Cooling Efficiency

The cooling efficiency in steady state is plotted in Figure 15and Figure 16. The graphs are given in terms of COP, instead of the more familiar cooling, mixed-unit, EER. To convert between the two, multiply COP by 3.412. Similar to heating, both models show high efficiencies across the temperature range. In general, the manufacturer's cooling ratings are in good agreement with our lab test results.

Figure 15. 12RLS COP Plot.

(Steady state lab data plotted as blue, red, and green points.)

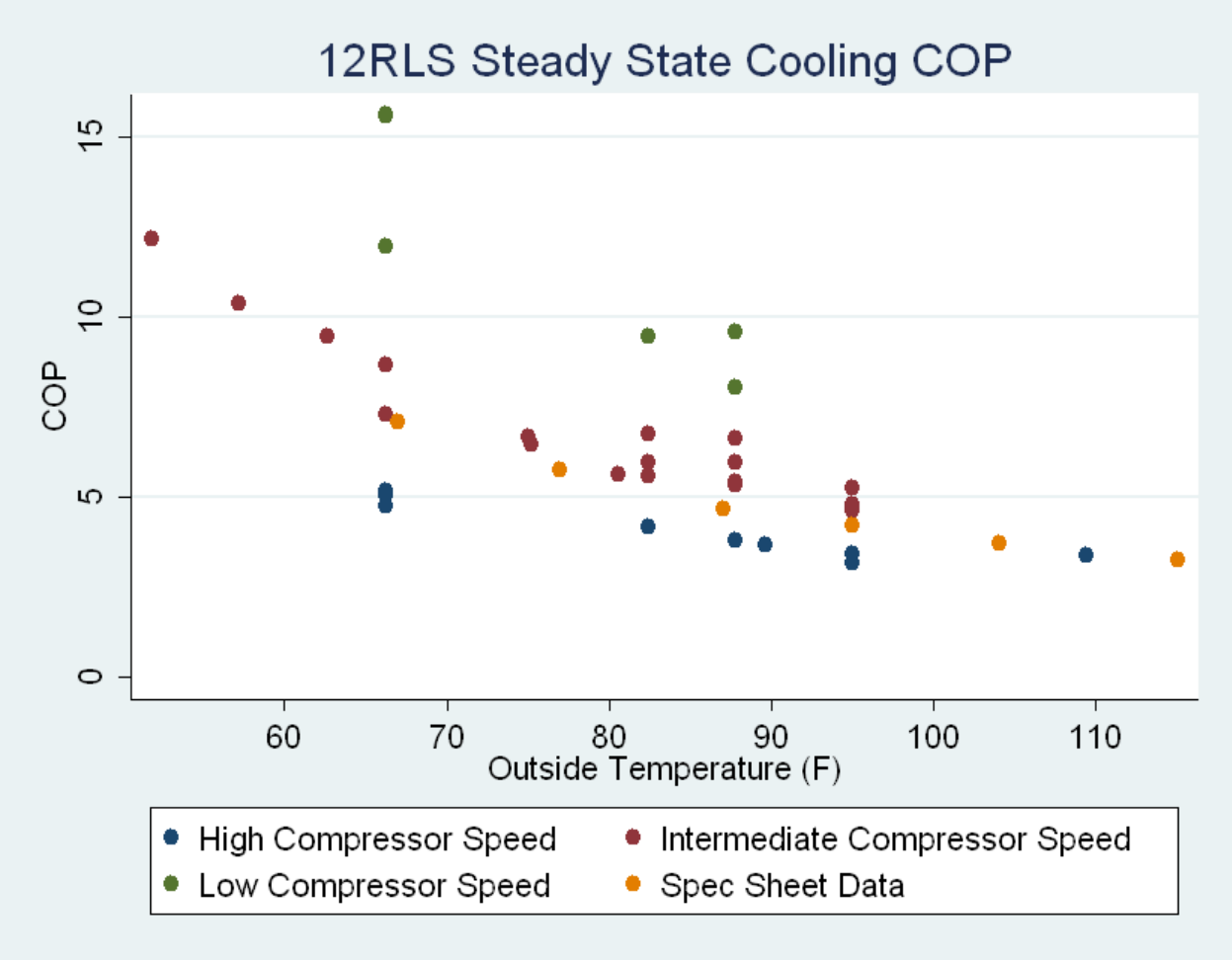

Figure 16. FE12NA COP Plot.

(Steady state lab data plotted as blue, red, and green points.)

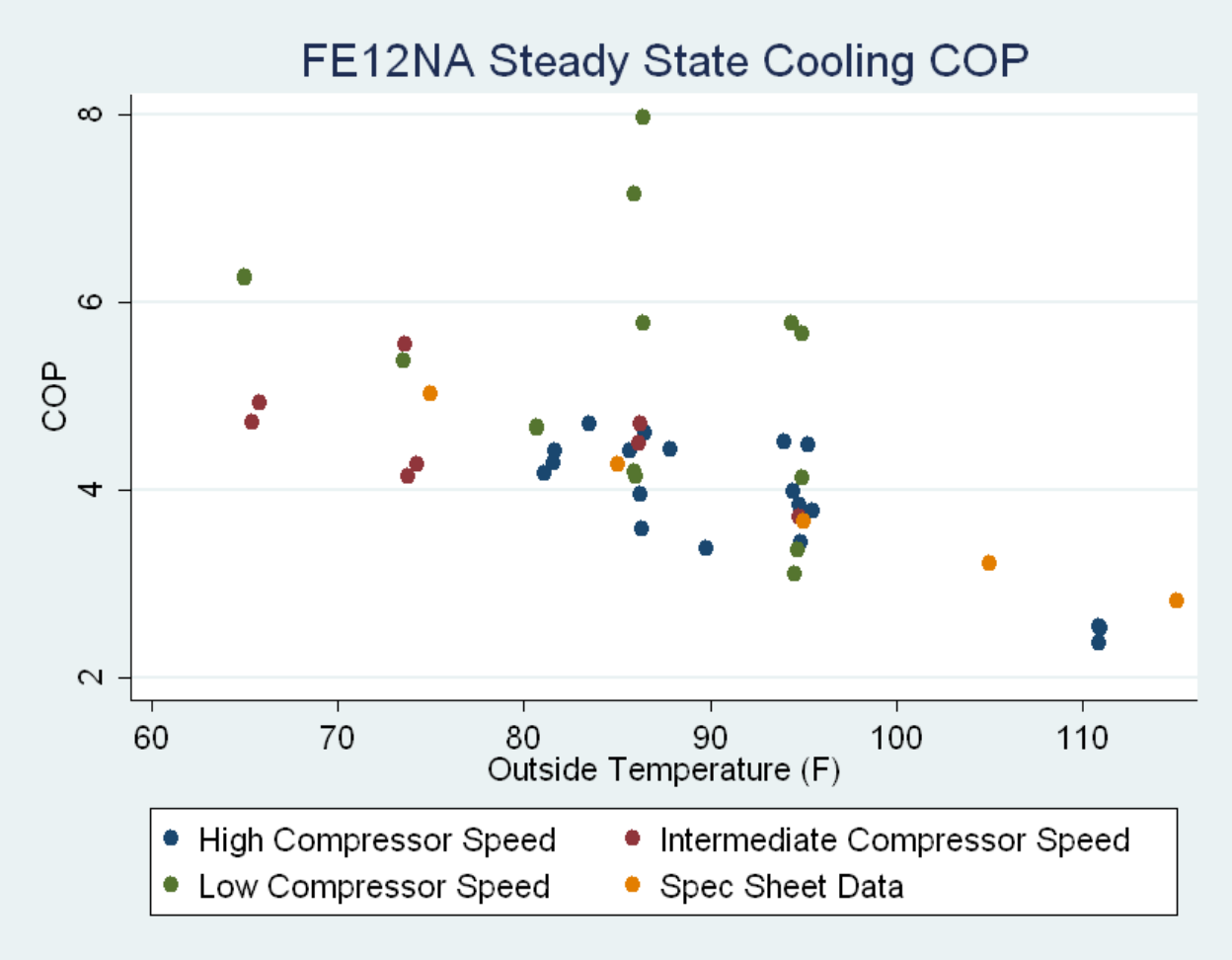

5.2. Cooling Mode Cycling

Two cycling tests were conducted for each DHP. The first was the AHRI 210/240 specified one which cycles the equipment from low power to off at 67°F outdoor temperature. A second test was added which cycles the equipment from high power to off at the same temperature to better understand the effects of cycling. The max load to off cycling demonstrated there is very little energy penalty to this type of cycling. Essentially, the equipment is well set up to switch on to a high fan and high power state. This was the same findings as in heating. For the low load cycling, there is still a noticeable energy penalty when compared to the equipment operating at steady state at that low load. When cycling on, the DHP targets an initially higher output than required and overshoots the optimal performance range.

The cooling cyclic degradation coefficient, Cd, was determined to be 0.43 for the 12RLS. The Cd for the FE12NA could not be determined due to testing challenges. Even with the manufacturer supplied controller, the lab could not replicate the required, paired steady-state and

cycling tests to determine Cd. For the cycling test, the FE12NA would cycle on but at a load lower than any observed in the steady-state test regime. Operating at this lower load will give a comparatively higher COP and thus results in a negative Cd. The lab made several attempts at the tests to confirm the challenges and then moved on to the over items in the test suite. In all SEER calculations, the default value of 0.25 is used for both equipment models instead of the measured value.

6. SEER and HSPF Ratings Evaluation

The lab testing plan called for conducting the full set of tests necessary in calculating SEER and HSPF ratings. The purpose of conducting the rating point tests was not to verify the manufacturer's rating but to understand the relationship between the ratings mandated by the federal standards and the performance of this equipment in a variety of load conditions. The other tests in the test suite create a detailed performance map that far surpasses any single rating. Therefore, these can be used as a baseline comparison for equipment performance to the rating tests.

The AHRI 210/240 testing and rating procedures call for several tests at different rating conditions which are then weighted together to derive a single rating. This procedure was designed in the 1980s to rate single speed compressors in split systems. With the advent of widely available variable speed equipment, the test standard was expanded to include specific tests and a specific section on the calculation procedure for those systems. While the weighting scheme may have limitations for single speed technology, its use in the variable speed compressors and fan systems of the DHP requires that the tests be restricted to operating conditions and control points that are arbitrary. In effect, the equipment could have a wide variety of ratings depending on the testing and control decisions made during the testing process.

One important finding is learning how challenging it is to replicate the ratings for variable speed equipment. There are a total of eight heating tests and seven cooling tests which must be exactly replicated if one expects to match literature data. Further, the critical values in the rating calculation come from "intermediate" speed compressor operation. The intermediate speed is generally the basis for nominal input, output, and COP at a particular testing temperature. All of the mid-range points plotted in Figure 5, Figure 6, Figure 13, and Figure 14 demonstrate the DHPs have multiple of what can be considered intermediate operating conditions in the compressor and several in the fan. Deviations from the exact intermediate values will lead to differences in output calculations, which is what we encountered. Much of the difference may be traced to decisions of what would be considered representative control points.

To consistently create an intermediate operating speed for purposes of lab testing, manufacturers generally have a special controller which sets and maintains a specific operation. The device is external to the DHP and designed to be used in the rating process. At the start of testing, both manufacturers were queried about obtaining and using the controller in the project. The controller for the FE12NA was obtained and used while the one for the 12RLS was not.

Surprisingly, it was easier to replicate the 12RLS results without a controller. Even with the manufacturer's controller for the FE12NA, the equipment could not be coaxed into a critical, intermediate test point for use in the HSPF calculation. Several attempts were made before testing priorities, such as completing the full performance map, and time constraints necessitated the need to move on.

The calculation of the HSPF for the 12RLS showed agreement with the catalog value, while the HSPF for the FE12NA did not agree. The first approach at the FE12NA HSPF calculation was made using the measured, $H1_1$ and $H2_V$ test points[10], which gave an unreasonably low result due to difficulties in observing the DHP at the proper compressor speed. Therefore, the second, and final approach, used simulated data points for these two tests from the performance model to calculate the HSPF value which proved to be a much higher result. The results are given in Table 5. The data should not be taken as an official result in part because of the simulated data point used.

Neither of the measured SEER values agreed with the catalog data and both were lower. This is somewhat expected as previous Ecotope work on three single speed heat pump showed lower measured SEER values (Kruse 2006, Kruse 2008, Palmiter 2011). The earlier work showed values roughly one point lower while all but one of these are substantially lower. It should be pointed out that the EER, rather than SEER, which is influenced by humid test conditions, is more indicative of energy performance in the Pacific Northwest with its dry, almost completely sensible cooling climate.

Table 5. HSPF and SEER Calculation Results.

(HSPF Zones are defined in the 210/240 Std. Zone 1 is the warmest; 5 is the coldest. Zone 6 is for marine climates. Only Zone 4 HSPF is required to be published and printed on the equipment label.[11])

		12RLS	FE12NA*
Heating HSPF by Zone	1	15.2	10.4
	2	14.6	10.3
	3	13.8	10.1
	4	11.8 [12]	9.3 [10.6]
	5	8	7.1
	6	15.8	10.6
Cooling SEER		20.3 [25]	15.5 [23]
Cooling EER		11.4 [14.46]	10.9 [12.9]

[bracketed] number indicates catalog value.

*All HSPF values calculated using simulated $H1_1$ $H2_V$ tests.

Because of the challenges encountered in testing, these results do not definitively demonstrate higher or lower performance than the catalog data. As discussed above, one major reason for the disagreement of the values is due to the intermediate speed operating points which were difficult to replicate. It is likely that the compressor speeds used in the lab for generating these data

[10] See AHRI 210/240 for definition of $H1_1$ and $H2_V$ test conditions.

[11] See Francisco, Palmiter and Baylon 2004 for a discussion of HSPF zones

points were higher than those used by the manufacturer. The use of a higher speed would lead to lower efficiencies and hence a lower HSPF and SEER rating. Another possibility for the difference is the tolerance allowed in the testing conditions which is a ±2°F variation in both the indoor and outdoor dry bulb temperatures. A tightly controlled thermal chamber could be set to operate at the optimal ends of the tolerance range and produce better rating results.

Another source of the discrepancy could be due to ambiguities in the calculation procedure itself. For example, the HSPF calculation requires the input of a temperature where the heat pump stops operating and where resistance heat would take over. Guidance is not given in the standard on what to use in this case since there is no electric element in the DHPs tested. We elected to use field data collected at several sites which encountered very low outside temperatures. This resulted in a direct observation of the controller's response to the cold temperatures and to the increased load that the house experienced during these temperatures.[12]

For the SEER calculation, there is an undefined temperature input value,[13] used to determine the efficiency across a range of compressor speeds and temperatures. Its meaning can be inferred from other parts of the calculation procedure but a clear definition would remove the ambiguity. As with the HSPF testing we referred to the operating characteristics we could observe in the field for guidance which allowed a better sense of compressor speeds during high temperature cooling events. Unfortunately, it does not appear that either manufacturer's SEER rating is well represented by our testing.

[12] For further clarification, the lowest value for the design heating requirement, DHR, in the HSPF calculation was used per Energy Conservation Program for Consumer Products: Test Procedure for Residential Central Air Conditioners and Heat Pumps. 10 CFR Part 430. (2005).

[13] The temperature variable in question is T_2. AHRI Std 210/240-2008, page 97, Section 4.1.4.1. Inferred to mean temperature at which the compressor, operating at maximum speed, matches the building load.

7. Performance Model Development

7.1. Overview

One of the main goals of the lab evaluation was to collect enough data to develop a set of equipment performance models. The performance models are intended to be used in simulation programs as predictive tools to determine how much energy a DHP would use on an annual basis.

The foundation of the model is based on the performance map of the steady-state data. The steady state data describes how the equipment would operate in an idealized, constant load situation. From there, the steady state performance is modified with additional factors and curve fits to account for on/off cycling, defrost cycles, and responses to load/set point changes. Additionally, in simulation software, for applications where the DHP shares the heating load with another system (as is the case in this pilot study), the program needs to account for the interaction of the two systems. This report mainly deals with the performance curve fits and models of the DHP only. Field data, which are being collected in other parts of the pilot project, are needed to determine how to couple the two heating systems together.

For this project, the performance model is being developed for use with SEEM (Simple Energy and Entropy Model)[14] although any simulation software could use the curve fits. In the simulation, SEEM will "request" the needed output capacity from the performance model. This approach differs from single-speed equipment which has a fixed capacity as a function of temperature. Instead, SEEM checks if the needed capacity is within the realm of possible for the equipment and then determines the required power input to generate that output. In a situation where the DHP is sharing the house load, some a priori assumption is likely needed to determine which fraction of the house heating load the DHP could satisfy. SEEM would then request this fractional capacity from the performance model.

The performance curves for the DHPs are formulated as functions of equipment load, outdoor temperature and RH, indoor temperature and RH, and indoor unit airflow. The equipment load is used in the curve as a proxy for compressor speed. The heating model is the simplest case because it does not depend on indoor RH. Cooling will depend on indoor humidity and whether the indoor coil is wet or dry. The cooling model will also account for the split between sensible and latent capacities.

[14] SEEM was developed by Larry Palmiter at Ecotope to model heating and cooling energy use in small scale residential structures. The program consists of an hourly thermal and moisture (humidity) simulation that interacts with duct specifications, equipment, and weather parameters to calculate the annual energy requirements of the building. It employs algorithms consistent with current ASHRAE, AHRI, and ISO calculation standards. SEEM is used extensively in the Northwest to estimate conservation measure savings for regional energy utility policy planners.

Herrick Labs developed full equipment performance models as well as useful parameterization techniques to deal with the variable speed nature of the compressor and fan. Ecotope employed some of the parameterization concepts and then independently developed a heating model. The cooling model used is the one developed by Herrick Labs. In all cases, regression techniques were used on the entire performance map of the measured data to create simplified functional fits.

7.2. Model

The model concepts are first explained briefly and then developed in more detail below. The model is intended to be used in the following way:

- Calculate maximum output capacity, Q_{max} (Eqn 1), and maximum input power, W_{max} (Eqn 2) at the given indoor and outdoor conditions using a fitted curve from equations 1 and 2.
- Using the load requested from the simulation, Q, determine at what fraction of capacity the compressor is operating: Q/ Q_{max} and $(Q/ Q_{max})^2$
- Using the airflow value supplied by the simulation, CFM,[15] and the capacity, Q, calculate Q/CFM. The model then checks the capacity to flow ratio against a maximum allowed value to insure the simulation is not trying to ask for an unrealistically high capacity with a low flow. The parameterization and values for Q/CFM are derived from the lab tests themselves.
- Calculate the predicted power input, $W_{predicted}$, that is needed to generate the requested capacity at the selected airflow under the specific ambient air conditions (Eqn 3).
- If the load is low and the equipment is cycling, applying a cycling factor correction.
- If the ambient conditions are in a frosting regime, applying a defrost factor correction.

The first step in developing the model is to determine the maximum input power and output capacity across all temperatures. These curve fits are plotted in Figure 11 for heating. The fits are given in the equations below and the coefficients in Table 6 and Table 7. All temperatures are input in °F; Qmax, the output capacity, is output in Btu/hr; and Wmax, the input power is output, in W. Equations 1 and 2 capture both the indoor and outdoor temperature dependence.

$$Q_{max} = q_{rate}*[qb0 + qb1*T_{out} + qb2*T_{out}^2 + qb8*(T_{in}-70)/(70-T_{out})] \quad \text{(Equation 1)}$$

$$W_{max} = w_{rate}*[wb0 + wb1*T_{out} + wb2*T_{out}^2 + wb8*(T_{in}-70)/(70-T_{out})] \quad \text{(Equation 2)}$$

[15] The airflow value is either a user input, fixed value, or function designed to operate the equipment at optimum efficiency.

Table 6. Maximum Output Capacity Curve Fit Coefficients.

(The r^2, goodness of fit, value is also given in the table.)

	12RLS	FE12NA
r^2	0.91	0.99
q_{rate}	20587	19580
qb0	0.6890756	0.4413528
qb1	0.0088316	0.0209345
qb2	-0.0000440	-0.0001815
qb8	-0.0526629	-0.1584849

Table 7. Maximum Power Input Curve Fit Coefficients.

(The r^2, goodness of fit, value is also given in the table.)

	12RLS	FE12NA
r^2	0.91	0.79
w_{rate}	1925	2226
wb0	1.05754	0.6432956
wb1	0.0064188	0.013828
wb2	-0.000137	-0.0001534
wb8	0	-0.0870158

Using these max value curves from equations 1 and 2, both the input power and output capacity are parameterized as fractions of the maximum value. The max value curves are also used in the simulation to bound the upper limit of output provided by the DHP.

To capture the airflow performance dependence, we introduce another term which is the ratio of the capacity to the airflow, Q/cfm. With the ratio of desired capacity to maximum capacity, and the capacity to airflow, the power input required can be predicted using Equation 3 and Table 8.

$$W_{predicted} = W_{max} * [d0 + d1*(Q/Q_{max}) + d2*(Q/Q_{max})^2 + d11*(Q/cfm)] \qquad \text{(Equation 3)}$$

Table 8. Curve Fit Coefficients to Predict DHP Input Power.

(Use with Equation 3.

The r^2 values are also given which demonstrate overall model fit to measured data.)

	12RLS	FE12NA
r^2	0.97	0.89
d0	-0.1228436	-0.2208177
d1	0.6949213	1.051991
d2	0.3444927	0
d11	0.0016292	0.0037269

The lab results showed that changing the indoor fan speed setting, from low, medium, or high, changed the performance. The higher the airflow, the better the heat transfer across the indoor coil, so both capacity and efficiency increase. As the airflow increases, so does the power needed to run the fan (typically 20W from low to high), but the efficiency gains in heat transfer make up for the added power. Conversely, for a given output capacity, as the airflow decreases, the compressor has to work harder in order to raise the supply air temperature. This comes as a performance penalty. Instead of separating fan power in the model, we rolled it into the total power.

To complete the heating model, several more parameters are needed, including a maximum allowable capacity per unit airflow, the cycling degradation coefficients, and a minimum low load limit. These are given in Table 9.

Empirically, each piece of equipment was determined to have a maximum capacity per unit airflow, $Q/CFM|_{max}$. This is because in practice, maximum capacity is achieved with maximum airflow not with minimum. A larger value of $Q/CFM|_{max}$ means the equipment can deliver more heating or cooling with less flow. The capacity to airflow ratio limit is necessary in the model to prevent nonphysical conditions from being specified. It explicitly prevents a DHP airflow from being set low and then requesting a large capacity. Inside a simulation, when this occurs, the control strategy could be to either increase the airflow level or limit the output capacity. The $Q/CFM|_{max}$ limit is distinct from the maximum equipment output capacity which is governed mostly by the outdoor temperature. For a given set of ambient and indoor conditions, $Q/CFM|_{max}$ limits the capacity for a fixed indoor fan speed.

Equipment cycling modeling turns out to be especially important in DHP retrofit applications where the DHP can share the space heating load with an existing system such as a resistance heater. If this heater is configured to provide heat concurrently with the DHP, the apparent load on the DHP will diminish causing it to cycle. This would conceivably happen at lower outside temperatures than if the DHP were simply heating the space on its own. Therefore, it is useful to think of heating cycling occurring at the load fraction (which changes as a function of temperature) corresponding to the minimum input power. The minimum continuously observed operating power is given as the Min Power Input in Table 9. For loads (and powers) below this, the unit will cycle on and off. A standard treatment of cycling similar to what is used in the AHRI 210/240 standard for calculating the HSPF is used in the model.

Table 9. Additional Modeling Parameters.

	Units	12RLS	FE12NA
$Q/CFM\|_{max}$	Btu/hr/CFM	55	65
Min Power Input	W	220	450
Cd	--	0.28	0.45

The impact of defrost on the performance still needs to be implemented. The defrost tests suggest a 5-10% decrease but long-term observations of the field data show the impact could be larger. The field data measurements show it is possible to observe the frequency, duration, and power use during a defrost cycle. Therefore, Ecotope plans to mine the field data for defrost impacts and incorporate those findings into the final performance curves.

7.3. Curve Fit and Model Example

The curve fits and performance model can be better understood through an example using a house with the following characteristics:

- House UA = 400 Btu/hr°F. 65°F balance point. House set point is 70°F.
- DHP assumed to heat 65% of house. Remaining 35% heated with resistance baseboards.
- Use 12RLS DHP
- Defrost not yet in model
- Low load cycling in model is included

Figure 17 shows the output capacity and input power for the example house from -5°F to 65°F outside temperature. The area in red represents the DHP while the area in blue represents the baseboard resistance heaters. The load on the house increases as the temperature drops. In response, the DHP (and the baseboard heaters) increase their output capacity.[16] Because the DHP is carrying only 65% of the load, some resistance heat is used at all temperatures. Physically, this could happen if the occupant desires heat in a bedroom while the DHP is located in the living room. The DHP can't always heat the far zone effectively so supplemental heat is needed.

As the capacity of the DHP increases, so does the required input power. Notice the curved shape to the input power graph which comes directly from Equation 3. The graphs also plot the maximum capacity and input power from equations 1 and 2 as orange lines. When the load required by the house meets the maximum possible DHP capacity, the capacity then remains at maximum (which happens near 5°F and below in this example). When the DHP output is maximized, but the house load is greater, the simulation fills in the missing capacity with more resistance heat. Near 45°F, there is another inflection point in the input power. Above this temperature, for this house configuration, the load on the DHP is low enough that the equipment begins to cycle. The input power increases but the capacity, which is driven by the house heating requirements, stays the same. At the low temperature end, when the defrost model is implemented, it will effectively decrease the maximum available capacity when frosting occurs and increase the relative input power requirement.

[16] In practice, the baseboard heaters do not increase their capacity. They have a fixed output. Instead, the heaters will cycle on and off for different periods of time. Alternatively, more heaters, in different parts of the house could turn or off as well.

Figure 17. Example of DHP Performance Curve and Resistance Heat Interaction in a Sample House.

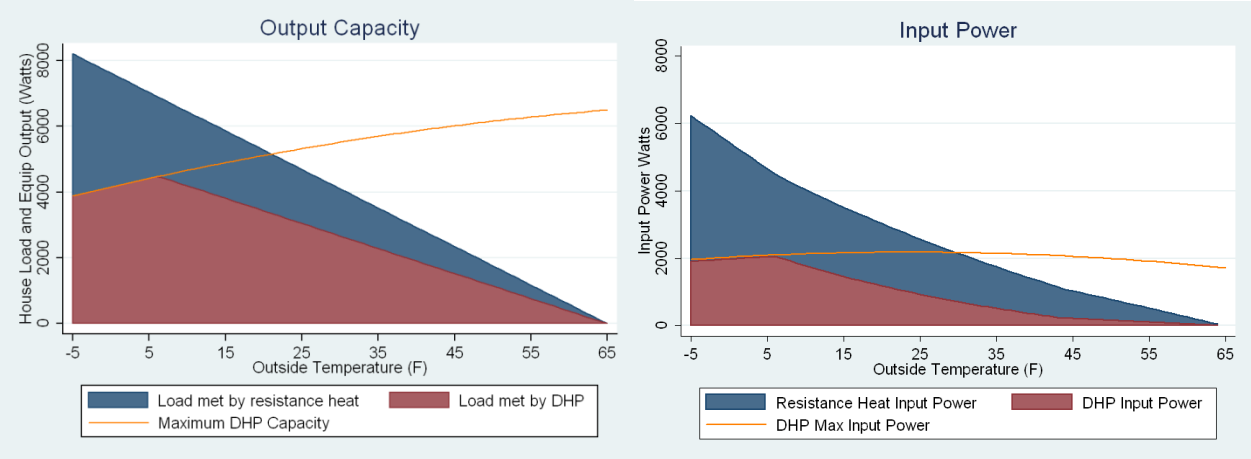

7.4. Cooling Model

The cooling performance model we elected to use was developed by Howard Cheung and Simbarashe Niyaka at Herrick Labs. Ecotope verified the workings of the model and was satisfied with its explanatory and predictive capability. It is attached in Appendix E where it is explained in detail.

8. Conclusions

The detailed performance mapping and subsequent analysis conducted in the lab testing of the 12RLS and FE12NA DHPs leads to several significant findings. They are described below.

- **The lab data demonstrates the high performance of both models.** The highly efficient operation will enable significant energy savings opportunities in both retrofit and new applications. Both equipment models have the potential to deliver on the promise of generous energy savings. Had the lab data revealed poor efficiency results, the ultimate energy savings estimates would be compromised. In the end, the savings achieved in a particular house will depend on a number of factors including the installation location within the building or the interaction with the existing heating system. Compressor and distribution efficiency of the DHP, however, will provide a strong foundation on which to build energy savings.

- **Lab and field COP measurements show good agreement.** The early analysis of the field data compares well to the lab measurements. Both measurements provide a useful cross reference for each other. The lab data is collected in a stable, repeatable, and highly controllable situation which provides a "reference set" for the field measurements of similar DHPs. Likewise, the field metering of COP shows which equipment operating modes are most common and therefore the most important parameters to measure in the lab. At the outset of the project, Ecotope did not anticipate the amount of synergy between the two data sets. It yields more confidence in both, while simultaneously demonstrating the benefits of an integrated evaluation approach to ductless heat pumps.

- **Both equipment models perform well at low outdoor temperatures.** Both models continue to operate well in cold temperatures with the 12RLS showing slightly higher capacity and efficiency. Installers and home-owners should be made aware that the equipment will continue to run and provide benefits at cold temperatures so that energy savings can be maximized.

- **The current HSPF and SEER ratings are not well suited to DHPs.** The testing standard and calculation procedure do not always produce ratings which characterize the performance of the equipment well or allow one to determine how the equipment might operate in a controlled environment like the lab, let alone a field installation. In lieu of the ratings, more data is needed to assess both the relative performance between models and the likely energy use of a single model. This data should include the typical operating speeds and compressor outputs that the equipment's controller uses to respond to heating conditions. Performance curves (including capacity and input power over a range of compressor loadings such as those developed in this project) and description of operational strategies will be useful in this regard. An updated testing procedure should include changes to the testing conditions, compressor speeds in particular, that make them more applicable to the way they perform in actual operation.

- **The equipment can be modeled in SEEM.** The performance model developed with the data collected in the lab will be implemented within SEEM. Importantly, the field data from the project will be integrated with the simulation to refine, calibrate, and validate

the model. The simulation will be appropriate to determine energy savings in both retrofit applications and new construction scenarios. This will allow the results of the lab testing and field data to be generalized to future evaluation of DHPs as a regional energy efficiency resource.

Lastly, the project demonstrates the value of an integrated approach to program evaluation. The simultaneous lab and field measurements reinforce one another. For example, the carefully measured indoor airflows in the lab were useful for calibrating the field measurements of output capacity and the subsequent equipment efficiency. Further, the field data showed which operating conditions were important to investigate in the lab. Finally, both will be combined to produce energy modeling tools.

Appendix A. Works Cited

Air-Conditioning, Heating, and Refrigeration Institute. (2008). Performance rating of unitary air-conditioning and air-source heat pump equipment, *AHRI Standard 210/240-2008* Arlington, VA. Air-Conditioning, Heating, and Refrigeration Institute.

American Society of Heating Refrigeration and Air-Conditioning Engineers. (2010). Methods of testing for rating seasonal efficiency of unitary air conditioners and heat pumps. *ASHRAE Standard 116-2010*.Atlanta, GA. American Society of Heating Refrigeration and Air-Conditioning Engineers.

American Society of Heating Refrigeration and Air-Conditioning Engineers. (1987). Standard Methods for Laboratory Airflow Measurement. *ASHRAE Standard 41.2-1987*.Atlanta, GA. American Society of Heating Refrigeration and Air-Conditioning Engineers.

Davis, B., Ecotope, Inc. (July 2009). Mini-split ductless heat pump bench test results. Prepared for Bonneville Power Administration. http://www.bpa.gov/energy/n/emerging_technology/pdf/BPA-Report_Ductless-Heat-Pump-June2009_FINAL.pdf

Energy Conservation Program for Consumer Products: Test Procedure for Residential Central Air Conditioners and Heat Pumps. 10 CFR Part 430. (2005). http://www1.eere.energy.gov/buildings/appliance_standards/residential/pdfs/cac_tp_101105.pdf

Geraghty, K., Baylon, D. & Davis, B. Ecotope Inc. (June 2009). *Residential ductless mini-split heat pump retrofit monitoring*. http://www.bpa.gov/Energy/N/doc/BPA-Report_Ductless-Heat-Pump-June2009.pdf

Francisco, P., Baylon, D., Davis, B., & Palmiter, L. (2004).Heat Pump System Performance in Northern Climates. *ASHRAE Transactions*, Volume 110, Part 1. American Society of Heating Refrigeration and Air-Conditioning Engineers. Atlanta, GA.

Fujitsu General Limited. (2009). *Design and Technical Data. Models: Indoor Unit ASU9RLS ASU12RLS Outdoor Unit AOU9RLS AOU12RLS*. Japan.

Fujitsu General Limited. (2009). *Service Instruction. Models: Indoor Unit ASU9RLS ASU12RLS Outdoor Unit AOU9RLS AOU12RLS*. Japan.

Kruse, E. & Palmiter, L. (2006). Measured Effect of Air Flow and Refrigerant Charge on Heat Pump Performance in Heating Mode. *ACEEE Summer Study on Energy Efficiency in Buildings.*

Kruse, E, Palmiter, L. & Francisco, P. (2008). Measured Effect of Air Flow and Refrigerant Charge on a High-Performance Heat Pump. *ACEEE Summer Study on Energy Efficiency in Buildings.*

Palmiter, L., Kim, J., Larson, B., Francisco, P., Groll, E., and Braun, J. (2011). Measured effect of airflow and refrigerant charge on the seasonal performance of an air-source heat pump using R-410a. *Energy and Buildings*. doi: 10.1016/j.enbuild.2011.03.026.

Mitsubishi Electric Corporation. (2009). *Indoor Unit Service Manual. Models MSZ-FE09NA MSZ-FE12NA*. No OBH542. Japan.

Mitsubishi Electric Corporation. (2009). *Outdoor Unit Service Manual. Models MUZ-FE09NA MUZ-FE12NA*. No OBH543. Japan.

Appendix B. Experimental Setup from Herrick Labs

Experimental setup: 12RLS

The Fujitsu 12RLS unit has an indoor unit and an outdoor unit that are installed in the corresponding rooms in the psychrometric chamber as shown in Figure 1 and Figure 2. A refrigerant circuit schematic diagram is shown in Figure 3.

Figure 1 Photo of the indoor unit with insulated discharge plenum

Figure 2 Photo of the outdoor unit

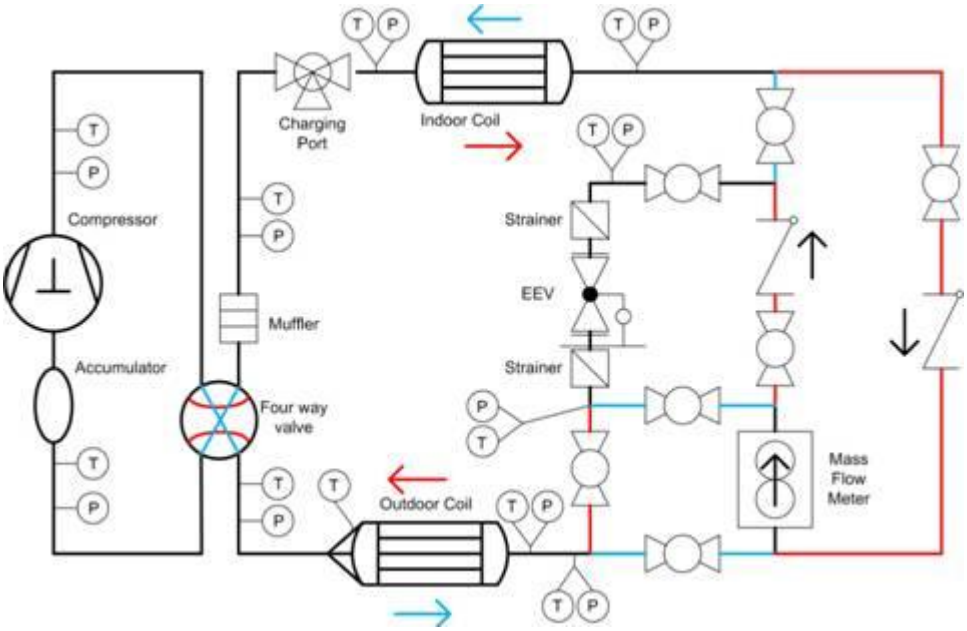

Figure 3 Refrigerant circuit schematic diagram

To characterize the refrigerant states, 11 OMEGA T-type thermocouples and 10 OMEGA PX32B1-2.5KAV millivolt pressure transducers are installed along the circuit ("T" and "P", respectively, in Figure 3). A system of valves allows the unidirectional Coriolis-type mass flowmeter to be used in both heating and cooling mode.

The system was initially charged with 1.25kg of R410a refrigerant for the heating mode tests. The recommended charge of 1.25kg gave zero subcooling for cooling mode operation which was unexpected. After consulting with Fujitsu on the expected subcooling values, the charge was increased to 1.52kg for all of the cooling tests. Three heating tests were conducted at both charge levels to ascertain if the higher charge value would alter the performance. Two of the tests showed a slightly higher heating capacity while one showed a lower heating capacity showing that the higher charge was on average 2.9% higher. The average difference is within the error bound of the measurement between refrigerant-side and air-side capacity so it was determined the added charge would not have had a measureable impact on the rest heating mode tests.

The air-side capacity of the indoor unit is computed using dry-bulb temperature, humidity, and airflow measurements on the indoor unit. Airflow is measured with a standard nozzle. An array of 9 T-type thermocouples on the inlet and 8 T-type thermocouples on the outlet are used to measure the average inlet and discharge air temperatures. The discharge plenum attached to the unit is insulated. Air flow is corrected for density, which is calculated from the humidity and temperature measurements made by a dew point sampling pump and 3 RTD sensors. Humidity at the inlet and outlet of the indoor unit was measured by a General Eastern Model SSM-1 humidity sampling pump. In each test, 10 minutes of stead-state dewpoint measurements were taken from one location. A toggle switch was then used to switch to the second location. Atmospheric pressure is measured by a mercury barometer, and power meters measure the total power to the indoor and outdoor units.

Data are collected at 10 second intervals and processed using an Agilent 34980A Multifunction Switch/Measure Unit and a Labview program generated specifically for this setup.

Experimental Setup FE12NA

Figure 4 and Figure 5 show the installation of the unit in the rooms of the psychrometric chamber. Refrigerant circuit schematics with refrigerant-side measurement points are shown in Figure 6, Figure 7 and Figure 8.

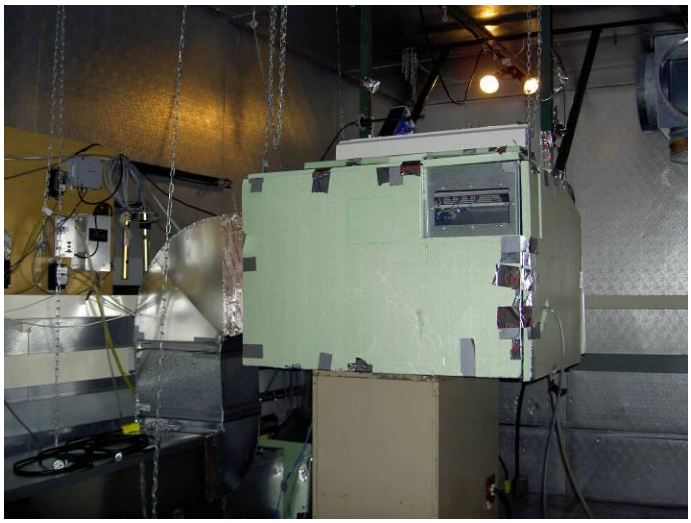

Figure 4 Photo of the indoor unit in the indoor room with insulated discharge plenum

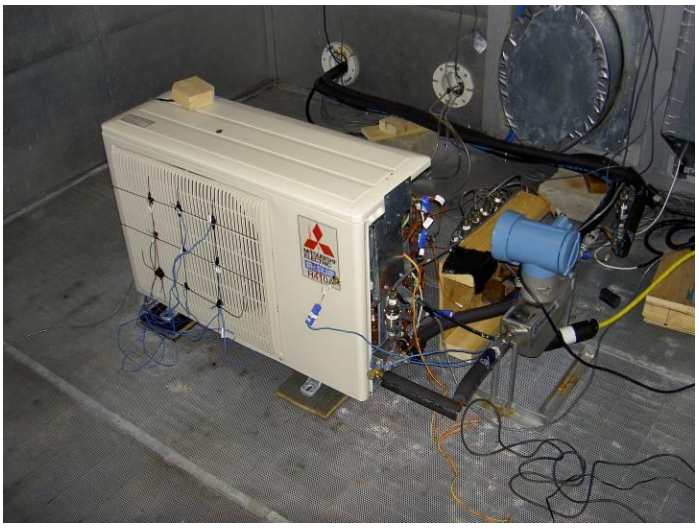

Figure 5 Photo of the outdoor unit in the outdoor room

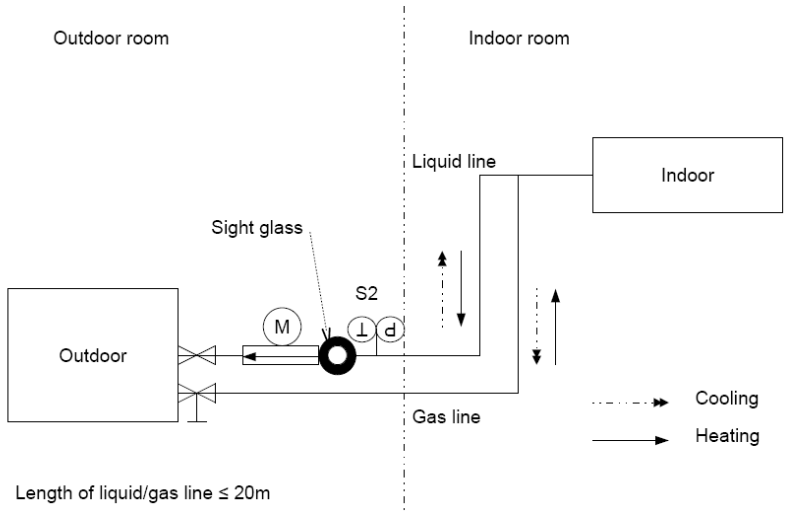

Figure 6 Overall refrigerant circuit schematic diagram

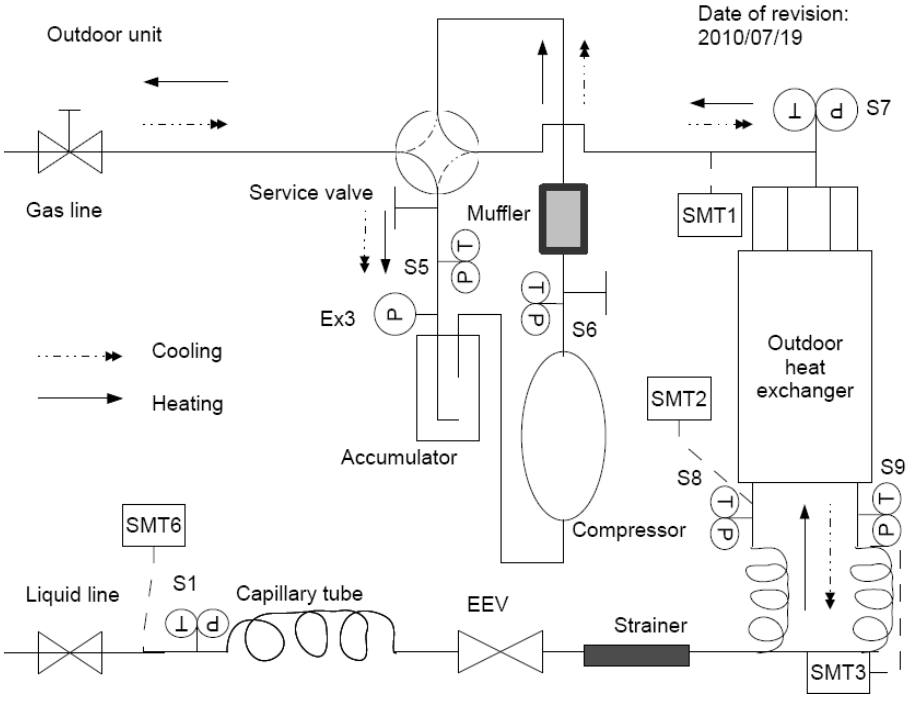

Figure 7 Refrigerant circuit schematic diagram of outdoor unit

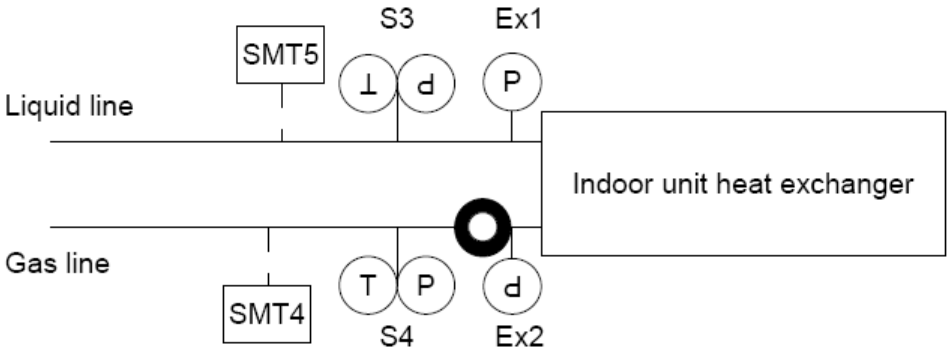

Figure 8 Refrigerant circuit schematic diagram of indoor unit

The states of refrigerant in the system were measured by 5 surface mounted OMEGA T-type thermocouples, 6 immersion OMEGA T-type thermocouples, 3 SETRA M207 pressure transducers and 9 OMEGADYNE PX32B1-2.5KAV millivolt pressure transducers ("S" for surface mounted thermocouple and OMEGADYNE pressure transducers, "EX" for SETRA pressure transducers and "SMT" for surface mounted thermocouples in Figure 6, Figure 7 and Figure 8. A Coriolis-type mass flowmeter measured the refrigerant liquid flow under heating operation. No refrigerant flow was measured in cooling operation because the liquid line piping at the condenser exit is too short for mass flow meter installation. The system was charged with 2.58lbs of R410a refrigerant for all tests.

The air-side capacity of the indoor unit was computed using dry-bulb temperature, humidity, and airflow measurements on the indoor unit. Airflow was measured with a standard nozzle. An array of 9 T-type thermocouples on the inlet and 8 T-type thermocouples on the outlet of the indoor unit were used to measure the average inlet and discharge air temperatures. Airflow was corrected for density at the nozzle as a function of the humidity and temperature measurements measured with a humidity sensor and 3 RTD sensors. Humidities at the inlet and outlet of the indoor unit were measured using two Vaisala HMP 230 sensors as shown in **Error! Reference ource not found.** and T-type thermocouples. A General Eastern Model SSM-1 dewpoint sampling monitor was used to measure the humidity at the air inlet of the outdoor unit. Atmospheric pressure was measured by a mercury barometer, and power meters measured the total power to the indoor and outdoor units.

Data were collected at 10 second intervals and processed using an Agilent 34980A Multifunction Switch/Measure Unit and an Agilent HPE1326B unit. A Labview program is also generated specifically for this setup.

Appendix C. Test Matrix

Tables of full test suite performed on Fujitsu 12RLS and Mitsubishi FE12NA.

12RLS Heating

Table 1 Test matrix for steady state tests

Test No.	Indoor Air		Outdoor Air		Indoor Fan Speed (rpm)	Number of tests at different compressor power
	Dry-Bulb (F)	Wet-Bulb (F)	Dry-Bulb (F)	Wet-Bulb (F)		
H-SS-62-H	70	<60	62	<56.5	1320 (Hi)	1
H-SS-62-M			62	<56.5	1130 (Me)	3
H-SS-62-L			62	<56.5	890 (Low)	3
H-SS-47-H			47	<43	1320 (Hi)	1
H-SS-47-L			47	<43	890 (Low)	2
H-SS-35-H			35	<33	1320 (Hi)	1
H-SS-35-M			35	<33	1130 (Me)	1
H-SS-35-L			35	<33	890 (Low)	1
H-SS-27-H			27	<25	1320 (Hi)	2
H-SS-27-M			27	<25	1130 (Me)	1
H-SS-17-H			17	<15	1320 (Hi)	2
H-SS-17-M			17	<15	1130 (Me)	1
H-SS-07-H			7	<6	1320 (Hi)	1
H-SS-N3-H			-3	--	1320 (Hi)	1

Table 2 Test matrix of cyclic test

Test No.	Indoor Air		Outdoor Air		Indoor Fan Speed (rpm)	Compressor speed range
	Dry-Bulb (°F)	Wet-Bulb (°F)	Dry-Bulb (°F)	Wet-Bulb (°F)		
H-CY-62-H-MX	70	<60	62	<56.5	1320 (Hi)	Maximum
H-CY-62-L-MN	70	<60	62	<56.5	890 (Lo)	Minimum

Table 3 Test matrix for defrost test

Test No.	Indoor Air		Outdoor Air		Indoor Fan Speed (rpm)	Compressor speed range
	Dry-Bulb (°F)	Wet-Bulb (°F)	Dry-Bulb (°F)	Wet-Bulb (°F)		
H-DF-35-M	70	<60	35	33	1130 (Me)	Maximum
H-DF-17-M	70	<60	17	15	1130 (Me)	Maximum

Table 4 Test matrix for morning warm-up test

Test No.	Indoor Air		Outdoor Air		Indoor Fan Speed (rpm)	Compressor speed range
	Dry-Bulb (°F)	Wet-Bulb (°F)	Dry-Bulb (°F)	Wet-Bulb (°F)		
H-MW-47	64 → 70	<60	47	<43	890 (Lo)	Default
H-MW-35	64 → 70	<60	35	<33	1130 (Me)	Default

12RLS Cooling

Table 5 Cooling Steady State Test Matrix

Test no.	Outdoor condition		Indoor condition		Indoor fan	Compressor
	Dry Bulb Temp (°F)	Wet Bulb Temp (°F)	Dry Bulb Temp (°F)	Wet Bulb Temp (°F)		
C-SS-110-H-MX	110	Dry coil	80	67	Hi	Maximum
C-SS-095-H-MX	95				Hi	Maximum
C-SS-095-M-MX					Me	Maximum
C-SS-095-M-INT						Intermediate
C-SS-095-L-MX					Lo	Maximum
C-SS-095-L-INT						Intermediate
C-SS-095-L-MN						Minimum
C-SS-090-H-MX	90				Hi	Maximum
C-SS-087-H-MX	87				Hi	Maximum
C-SS-087-H-INT						Intermediate
C-SS-087-M-MX					Me	Maximum
C-SS-087-M-INT						Intermediate
C-SS-087-M-MN						Minimum
C-SS-087-L-INT					Lo	Intermediate
C-SS-087-L-MN						Minimum
C-SS-082-H-MX	82				Hi	Maximum
C-SS-082-M-MX					Me	Maximum
C-SS-082-M-INT						Intermediate
C-SS-082-L-INT					Lo	Intermediate
C-SS-082-L-MN						Minimum
C-SS-075-H-MX	75				Hi	Maximum
C-SS-067-H-MX	67				Hi	Maximum
C-SS-067-M-MX					Me	Maximum
C-SS-067-M-INT						Intermediate
C-SS-067-L-INT					Lo	Intermediate
C-SS-067-L-MN						Minimum
C-SS-067-H-MX-D				Dry coil	Hi	Maximum
C-SS-067-L-MN-D					Lo	Minimum

Table 6 Cooling Cycling State Test Matrix

	Outdoor condition		Indoor condition		Indoor fan	Compressor
Test no.	Dry Bulb Temp (°F)	Wet Bulb Temp (°F)	Dry Bulb Temp (°F)	Wet Bulb Temp (°F)		
C-CY-067-H-MX-D	67	Dry coil	80	Dry coil	Hi	Maximum
C-CY-067-L-MN-D					Lo	Minimum

Table 7 Test matrix for evening cool-down tests

	Outdoor condition		Indoor condition		Indoor fan
Test no.	Dry Bulb Temp (°F)	Wet Bulb Temp (°F)	Dry Bulb Temp (°F)	Wet Bulb Temp (°F)	
C-ED-095-M	95	Dry coil	80	67	Me
C-ED-082-L	82				Lo

FE12NA Heating

Table 8 Heating steady state test matrix

Test code	Indoor temperature (°F)	Outdoor temperature (°F)	Fan speed	Compressor speed
H-SS-62-H-MX	70	62	High	Maximum
H-SS-62-H-MN	70	62	High	Minimum
H-SS-62-M-MX	70	62	Med	Maximum
H-SS-62-M-INT	70	62	Med	Intermediate
H-SS-62-L-MX	70	62	Low	Maximum
H-SS-62-L-MN	70	62	Low	Minimum
H-SS-47-H-MX	70	47	High	Maximum
H-SS-47-L-INT	70	47	Low	Intermediate
H-SS-47-L-MN	70	47	Low	Minimum
H-SS-35-H-MX	70	35	High	Maximum
H-SS-35-M-INT	70	35	Med	Intermediate
H-SS-27-H-MX	70	27	High	Maximum
H-SS-27-H-MN	70	27	High	Minimum
H-SS-27-M-INT	70	27	Med	Intermediate
H-SS-27-L-MN	70	27	Low	Minimum
H-SS-17-H-MX	70	17	High	Maximum
H-SS-17-M-MX	70	17	Med	Maximum
H-SS-17-M-INT	70	17	Med	Intermediate
H-SS-7-H-MX	70	7	High	Maximum

H-SS-n3-H-MX	70	-3	High	Maximum
H-SS-35-M-MX	70	35	Med	Maximum
H-SS-7-L-MX	70	7	Low	Maximum
H-SS-62-H-MX-75	75	62	High	Maximum
H-SS-62-H-MX-60	60	62	High	Maximum
H-SS-47-H-MX-75	75	47	High	Maximum
H-SS-47-H-MN-75	75	47	High	Minimum
H-SS-47-L-INT-75	75	47	Low	Intermediate
H-SS-35-M-INT-64	64	35	Med	Intermediate
H-SS-35-H-MX-60	60	35	High	Maximum
H-SS-27-H-MX-75	75	27	High	Maximum
H-SS-27-H-MX-60	60	27	High	Maximum

Table 9 Heating Cycling test matrix

Test code	Test method	Indoor temperature (°F)	Outdoor temperature (°F)	Fan speed	Compressor speed
H-CY-62-H-MX	Cyclic	70	62	High	Maximum
H-CY-62-L-MN	Cyclic	70	62	Low	Minimum

Table 10 Test matrix for defrost test

Test code	Indoor temperature (°F)	Outdoor temperature (°F)	Fan speed	Compressor speed
H-DF-17-M	70	17	Med	Maximum
H-DF-35-M	70	35	Med	Maximum
H-DF-47-M	70	47	Med	Maximum

FE12NA Cooling

Table 11 Cooling Steady State Test Matrix

Test code	Indoor dry-bulb temperature (°F)	Indoor wet-bulb temperature (°F)	Outdoor temperature (°F)	Fan speed	Compressor speed
C-SS-110-H-MX	80	67	110	High	Maximum
C-SS-095-H-MX			95	High	Maximum
C-SS-095-H-MX-76		76		High	Maximum
C-SS-095-H-MX-65		65		High	Maximum
C-SS-095-H-MX-85-D	85	Dry coil		High	Maximum
C-SS-095-H-MX-70-D	70			High	Maximum

C-SS-095-M-MX	80	67		Medium	Maximum
C-SS-095-M-INT				Medium	Intermediate
C-SS-095-L-MX				Low	Maximum
C-SS-095-L-INT				Low	Intermediate
C-SS-095-L-MN				Low	Minimum
C-SS-090-H-MX				High	Maximum
C-SS-087-H-MX			87	High	Maximum
C-SS-087-H-INT				High	Intermediate
C-SS-087-M-MX				Medium	Maximum
C-SS-087-M-MX-75-D	75	Dry coil		Medium	Maximum
C-SS-087-M-INT	80	67		Medium	Intermediate
C-SS-087-M-MN				Medium	Minimum
C-SS-087-L-INT				Low	Intermediate
C-SS-087-L-MN				Low	Minimum
C-SS-082-H-MX			82	High	Maximum
C-SS-082-M-MX				Medium	Maximum
C-SS-082-M-INT				Medium	Intermediate
C-SS-082-L-INT				Low	Intermediate
C-SS-082-L-MN				Low	Minimum
C-SS-082-M-MX-62		62		Medium	Maximum
C-SS-075-H-MX		67	75	High	Maximum
C-SS-075-L-INT-D		Dry coil		Low	Intermediate
C-SS-075-L-INT-58		58		Low	Intermediate
C-SS-067-H-MX		67	67	High	Maximum
C-SS-067-H-MX-72		72		High	Maximum
C-SS-067-H-MX-65		65		High	Maximum
C-SS-067-H-MX-85-D	85	Dry coil		High	Maximum
C-SS-067-H-MX-70-D	70			High	Maximum
C-SS-067-M-MX	80	67		Medium	Maximum
C-SS-067-M-INT				Medium	Intermediate
C-SS-067-L-INT				Low	Intermediate
C-SS-067-L-MN				Low	Minimum
C-SS-067-H-MX-D		Dry coil		High	Maximum
C-SS-067-L-MN-D				Low	Minimum

Table 12 Cooling Cycling Test Matrix

Test code	Indoor dry-bulb temperature (°F)	Indoor wet-bulb temperature (°F)	Outdoor temperature (°F)	Fan speed	Compressor speed
C-CY-67-H-MX	80	Dry coil	67	High	Maximum
C-CY-67-L-MN	80			Low	Minimum

Appendix D. Additional Heating Mode Graphs

Figure D1.

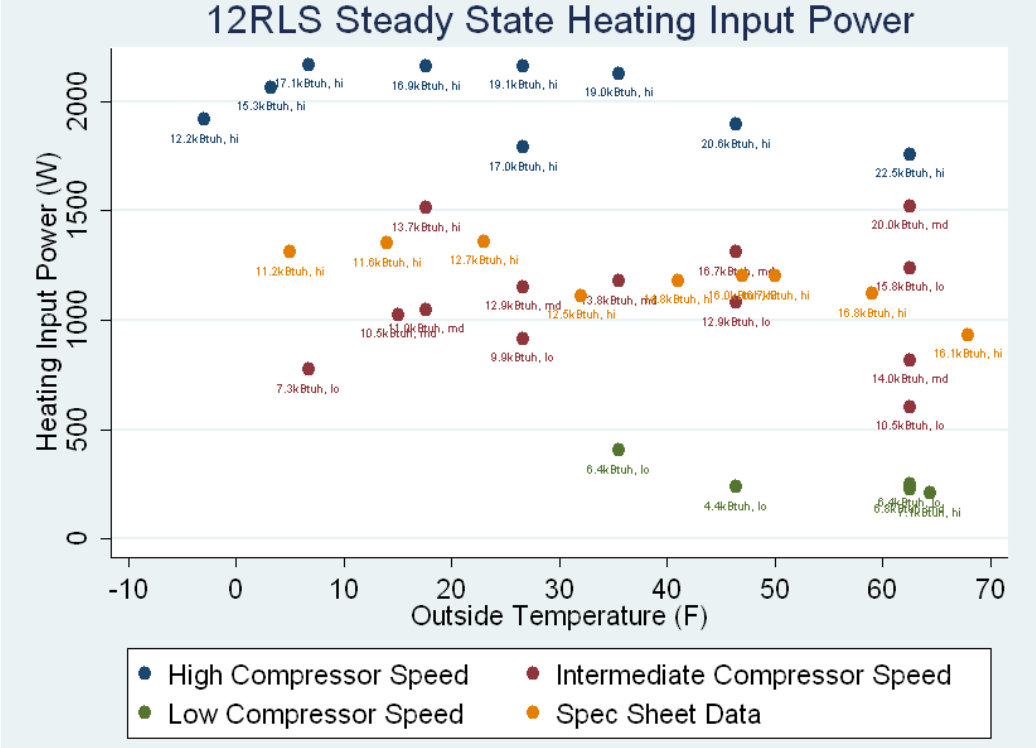

Figure D2.

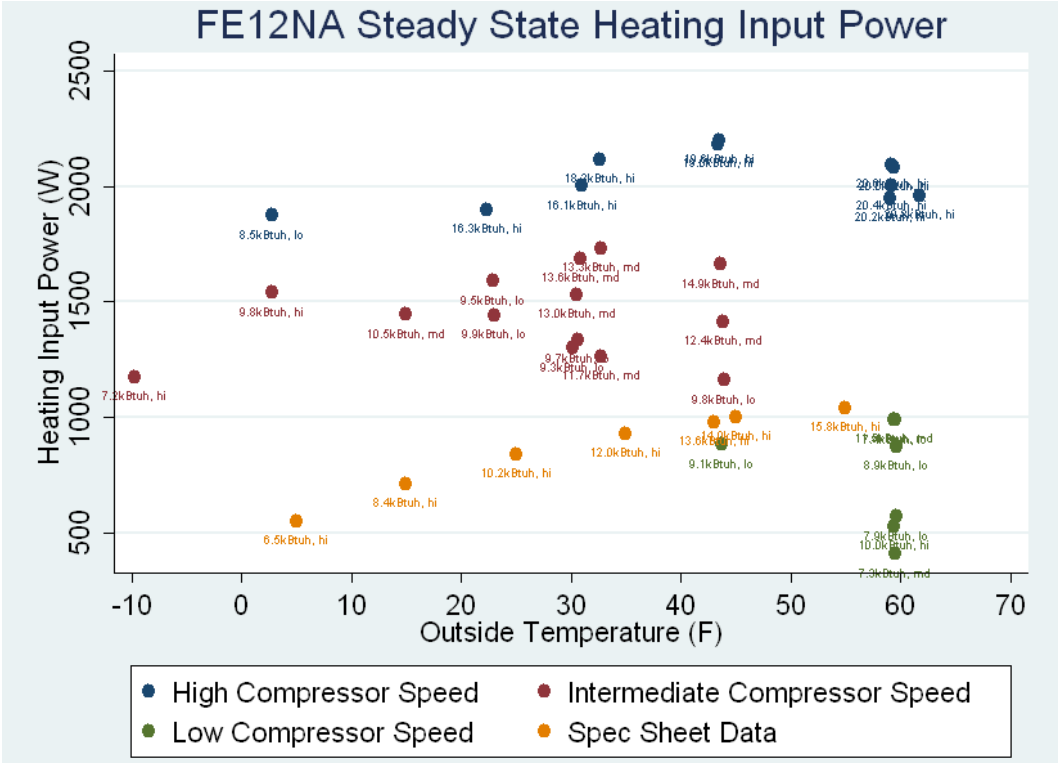

Appendix E. Heating and Cooling Model from Herrick Labs

What follows is the heating and cooling model developed by Herrick Labs from the measured data. Both Howard Cheung and Simbarashe Nyika worked to develop the model and should be credited where ever it is used. Ecotope independently developed a heating mode model which was presented in the main body of the report. The Herrick Labs heating mode model is given here for comparison purposes for the interested reader.

Excerpted from Monthly Progress report for February 2011:

1. Model consolidation and improvement

During this past month, additional work has been performed in developing a more general empirical modeling approach for DHP performance that works well for both the Fujitsu 12RLS and Mitsubishi FE12NA units. The indoor unit power consumption, the sensible heat ratio (SHR) and the total power consumption of the unit are characterized using empirical relationships that are described in this section. The new test results will be uploaded to the server.

The indoor unit power consumption is dominated by fan electricity and is assumed to be a quadratic function of indoor unit airflow as shown by equation (1).

$$W_{in} = g_0(V) = a_0 V^2 + a_1 V + a_2 \quad (1)$$

where

a_i is the i^{th} coefficient

W_{in} is the indoor unit power consumption

V is the volumetric air flow rate

The coefficients in equation (1) were calculated using regression applied to the experimental data. The estimated coefficients of equation (1) are shown in Table 4. Comparisons of model and measurements are presented in the appendix.

Table 4 Coefficients for equation (1)

Model	Fujitsu 12RLS		Mitsubishi FE12NA	
Mode	Heating	Cooling	Heating	Cooling
a0 ($W/(m^3/s)^2$)	1521.2	1321.8	888.95	1321.9
a1 ($W/(m^3/s)$)	-226.87	-200.71	-2.0047	-108.19
a2 (W)	18.044	17.059	1.3398	6.6958
Coefficient of determination	0.9988	0.9959	0.9813	0.9909

A sensible heat ratio model was then built for each unit operating in cooling mode. The sensible heat ratio model is mainly based on the ASHRAE Secondary Toolkit [4]. Equations (2) to (7) form the basic model along with psychrometric routines.

$$h_{adp} = h_{ent} - \frac{h_{ent} - h_{lvg}}{1 - BF} \quad (2)$$

$$SHR = \frac{h(t_{ent}, w_{adp}) - h_{adp}}{h_{ent} - h_{adp}} \quad (3)$$

$$BF = e^{-Ntu} \quad (4)$$

$$BF = \frac{h_{lvg} - h_{adp}}{h_{ent} - h_{adp}} = \frac{w_{lvg} - w_{adp}}{w_{ent} - w_{adp}} \quad (5)$$

$$h_{adp} = h(\omega_{adp}, r = 1) \quad (6)$$

$$Q = \dot{m}_{lvg}(h_{ent} - h_{lvg}) \quad (7)$$

where

h_{adp} is the effective surface enthalpy
h_{ent} is the air-water mixture enthalpy at the air inlet
h_{lvg} is the air-water mixture enthalpy at the air outlet
BF is the bypass factor
SHR is the sensible heat ratio
t_{ent} is the dry-bulb air temperature at the air inlet
ω_{adp} is the effective surface humidity ratio
ω_{ent} is the humidity ratio at the air inlet
ω_{lvg} is the humidity ratio at the air outlet
Ntu is the number of transfer units
r is the relative humidity
Q is the load delivered by the unit
$\dot{m}_{lvg}$ is the air mass flow rate

Equations (2), (4), (5) and (6) were used to find the Ntu for a single rating condition (C-SS-095-H-MX[17]). The Ntu is assumed to be constant under other scenarios and equations (2), (3), (4), (6) and (7) are used to obtain the SHR in all other cases. The Ntu values determined for the two units are shown in Table 5 and the comparisons between values of SHR determined from measurements and model predictions are presented in Figure 6 and Figure 7.

Table 5 Ntu for SHR model

Model	Fujitsu 12RLS	Mitsubishi FE12NA
Ntu	4.098	2.26

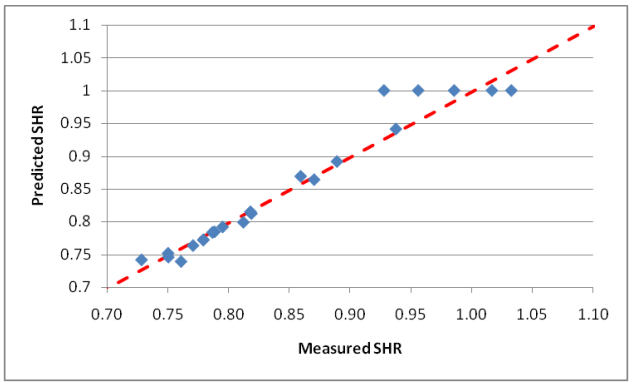

Figure 6 Fujitsu 12RLS SHR model performance

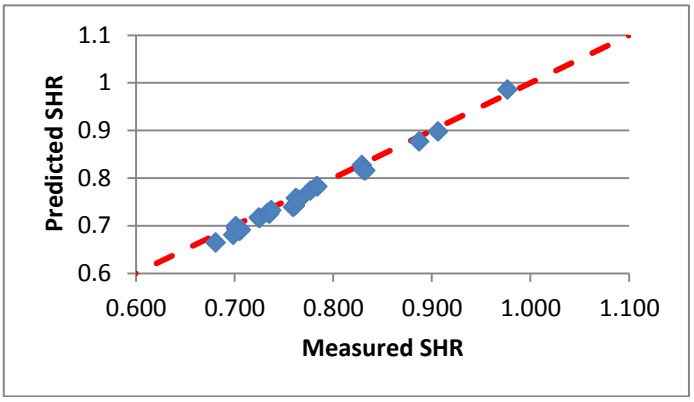

Figure 7 Mitsubishi FE12NA SHR model performance

[17] A steady-state test with outdoor dry-bulb temperature 95°F, indoor dry-bulb temperature 80°F, indoor wet-bulb temperature 67°F, high fan and maximum compressor speed.

The deviation in Figure 6 near unity SHR is a result of dry coil operation. Due to measurement uncertainties, dry conditions in experiments may be recorded to have SHR values less than one (or even higher than one). A predicted dry condition will give a unity SHR and will not provide values greater than unity.

The capacity and the power at capacity models capture the capacity and its power consumption at the highest indoor fan and compressor speeds at various conditions, resulting in expressions (8) and (9), dependent on environmental variables only.

$$Q_{max} = g_1(T_{amb}, T_{in}) \quad (8)$$

$$W_{max} = g_2(T_{amb}, T_{in}) \quad (9)$$

where

T_{in} is indoor coil inlet wet-bulb temperature in cooling and dry-bulb temperature in heating in °C

T_{amb} is the outdoor ambient dry-bulb temperature in °C

Q_{max} is the capacity in kW

W_{max} is the outdoor unit power consumption at Q_{max} in W

The expressions (8) and (9) are assumed to be quadratic as shown in equation (10). Regression was implemented on data with high indoor fan speed and maximum compressor speed to find the coefficients in the expressions.

$$g(T_{in}, T_{amb}) = b_0 + b_1 T_{amb} + b_2 T_{amb}^2 + b_3 T_{in} + b_4 T_{in}^2 + b_5 T_{in} T_{amb} \quad (10)$$

where b_i is the i^{th} coefficient in equation (10)

To obtain a compact and well-behaved performance model, backward elimination [5] was utilized to reduce the number of coefficients in (8) and (9) and a Matlab function *stepwisefit* was used to conduct the analysis. Initially, all regression coefficients in (10) were computed with the residual sum of squares of the model (Model I) recorded. Each coefficient, except the intercept, was removed one at a time from Model I and another residual sum of square (RSS) was recorded for each model with a removed coefficient (Model II). A partial F, given in equation (11), was calculated and the smallest among all Model II results is compared against an F-value[18] defined by a Type I error (α)[19] and the degree of freedom of residuals of Model I. Should the partial F be

[18] F-value is the F-statistic given by the F distribution, a kind of distribution function similar to normal distribution. F distribution is a distribution function to compare variances and hence degrees of freedom for both variances are needed for computation. For this project, the F-statistic is dependent on the numerator degree of freedom, 1, the denominator degree of freedom, ν, and the Type I error α

[19] α is the Type I error stating the probability of one hypothesis being accepted though the hypothesis is false in reality.

smaller than the F-value, the coefficient was eliminated and the Model II with the smallest F-value replaces Model I. The step was repeated by having another set of Model II based on the new Model I until the smallest partial F within the Model IIs was larger than the F-value. In this case, the Model I for this step was the final model. For this project, α was set to be 0.05.

$$\text{partial F} = \frac{RSS(\text{Model I}) - RSS(\text{Model II})}{RSS(\text{Model II})/\nu} \tag{11}$$

$$RSS = \Sigma(y_p - y_i)^2 \tag{12}$$

where

RSS is the residual sum of squares
ν is the degree of freedom of residuals of Model I = N – p – 1
y_p is the predicted value of the model
y_i is the measured value, in this case, Q_{max} and W_{max}
N is the total number of data
p is the number of coefficients

The coefficients and the coefficient of determination are tabulated in Table 6 and Table 7. Comparisons of measurements and predictions are provided in the appendix.

Table 6 Coefficients of (10) for Q_{max}

Model	Fujitsu 12RLS		Mitsubishi FE12NA	
Mode	Heating	Cooling	Heating	Cooling
b_0 (kW)	5.50517	2.28654	5.37617	2.5418364
b_1 (kW/°C)	0.12761	0.1692	0.24503	0
b_2 (kW/(°C)^2)	0	-0.0038	-0.0035	-0.002708
b_3 (kW/°C)	0	0.05686	0	0
b_4 (kW/(°C)^2)	0	0	0	-0.006535
b_5 (kW/(°C)^2)	-0.0036	0	-0.0075	0.010183

Table 7 Coefficients of (10) for W_{max}

Model	Fujitsu 12RLS		Mitsubishi FE12NA	
Mode	Heating	Cooling	Heating	Cooling
b_0 (W)	2050.971	-1420.2	1347.497	528.3236
b_1 (W/°C)	-11.8019	133.1013	91.64779	0
b_2 (W/(°C)^2)	-0.45836	-2.05742	-1.3067	0.157459
b_3 (W/°C)	2.310661	31.52992	37.60286	0
b_4 (W/(°C)^2)	0	0	0	-0.28755
b_5 (W/(°C)^2)	0	0	-3.81417	0.418263

The Mitsubishi unit exhibits a non-intuitive trend for capacity as a function of the temperatures, as demonstrated in Figure 8.

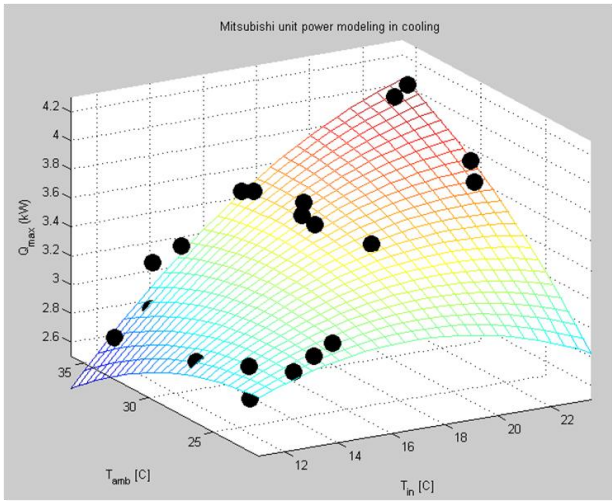

Figure 8 Mapping of capacity of Mitsubishi unit in cooling

At low ambient, the capacity decreases with increasing indoor wet bulb for values greater than about 18°C. The cause is the equipment safety algorithms that lead to auto-shutdown of the unit. When the indoor room temperature is higher than the ambient, the unit may switch off automatically. There is one data point at T_{in} = 22.31°C and T_{amb} = 23.49°C, but two other test points around this region experienced a continuous drop of capacity, followed by an auto-shutdown and operation in 10 minute on-off cycles. Care should be taken in applying the model for ambient temperatures below the indoor dry bulb temperature in cooling mode.

Typically, cooling capacity decreases with increasing ambient temperature. However, the capacity in Figure 8 actually increases with ambient temperature for high indoor wetbulb temperatures. The cause is also a consequence of a controller. A plot in Figure 9 helps to understand the reason.

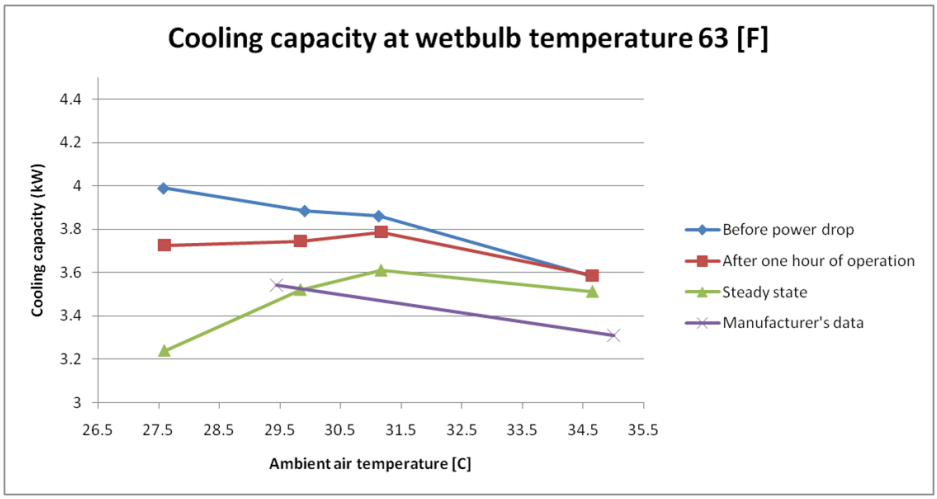

Figure 9 Capacity of Mitsubishi FE12NA at different times under 63°C indoor wet-bulb temperature and different ambient

During startup, the unit usually ramps up to a higher than normal compressor speed for that condition, leading to a relatively high outdoor unit power consumption for the first 30 minutes of operation. At the end of this initial startup period, the capacity shown in Figure 9 shows an expected trend: the higher the ambient, the lower the capacity. However, then the maximum compressor speed is reduced and the EEV controller adjusts the valve opening to maintain a discharge temperature from the compressor around 74°C. The lower the ambient temperature, the more that the EEV needs to close in order to maintain the discharge temperature setpoint. Throttling the refrigerant flow to maintain a relatively high compressor discharge temperature results in a significant capacity penalty at lower ambient temperatures. It is reasonable since low ambients require less capacity. However, it creates a trend that is quite different from systems which employ expansion valves controlling the superheat exiting the evaporator rather than the compressor discharge temperature.

In addition to the maximum heating or cooling capacity and associated power consumption, it is necessary to model the power consumption for a specified heating or cooling load requirement to provide a useful model for building simulation programs. The power consumption is a function of airflow and the required building load according the equation (13) to ensure that W_{total} equals to the sum of W_{max} and $W_{in}(V_h)$ when the building load equals to the capacity and V equals to V_h.

$$\frac{W_{total}}{W_{max}+W_{in}(V_h)} = d_1\left(\frac{Q}{Q_{max}} - 1\right) + d_2\left(\frac{V}{V_{max}} - \frac{V_h}{V_max}\right) + d_3\left(\frac{Q}{Q_{max}} - 1\right)^2 + d_4\left(\frac{V}{V_max} - \frac{V_h}{V_max}\right)^2 + d_5\left(\frac{Q}{Q_{max}} - 1\right)\left(\frac{V}{V_{max}} - \frac{V_h}{V_max}\right) + 1 \quad (13)$$

where

d_i is the i^{th} empirical coefficient in equation (13)
W_{total} is the power consumption of the unit
Q is the required building load
V_{max} is the highest airflow of the unit
V_h is the highest airflow for the given operation mode which may be different from V_{max}

Some of the coefficients in the equation (13) are eliminated based on the aforementioned backward elimination. The coefficients of the final equation, together with the coefficient of determination, are listed in Table 8. Other relevant diagrams can be found in the appendix.

Table 8 Coefficients in (13) and the coefficient of determination for different units in both cooling and heating

Model	Fujitsu 12RLS		Mitsubishi FE12NA	
Mode	Heating	Cooling	Heating	Cooling
d_1	1.6684	1.9918	1.1792	1.6580
d_2	0	0	0	0
d_3	0.5166	1.1113	0	0
d_4	0.6393	-0.1264	1.5487	0
d_5	0	0	-1.1758	1.2331
r^2	0.9948	0.9966	0.9835	0.9907

To use the model for cooling, cautions are needed for T_{in} in Q_{max} and W_{max} when the evaporator is dry. For modeling dry cooling, a hypothetical wet-bulb temperature that would result in a SHR of one according to the SHR model is needed. The hypothetical wet bulb temperature is used within the Q_{max} and W_{max} equations. A flow chart for the overall model is given in the appendix.

Table 9 to Table 11 provide limits on the operating range for the models based on the range of testing along with the safety and auto-shutdown conditions for the units.

Table 9 Applicable range of temperatures and important parameters for modeling

Model	Mode	Temperature	Minimum	Maximum
Fujitsu 12RLS	Heating	Indoor dry-bulb temperature [°C]	15.6	24
		Outdoor dry-bulb temperature [°C]	-14	17
Fujitsu 12RLS	Cooling	Indoor wet-bulb temperature [°C]	19	22.09
		Outdoor dry-bulb temperature [°C]	19	43.33
Mitsubishi FE12NA	Heating	Indoor dry-bulb temperature [°C]	13.82	23.53
		Outdoor dry-bulb temperature [°C]	-16.23	15.98
Mitsubishi FE12NA	Cooling	Indoor wet-bulb temperature [°C]	11.47	23.25
		Outdoor dry-bulb temperature [°C]	21.66	35.3

Table 10 Values for V_h and V_{max} in (13) for different models

Model	Mode	Airflow	Value
Fujitsu 12RLS	Heating	V_h [m3/s]	0.1975
		V_{max} [m3/s]	0.2138
Fujitsu 12RLS	Cooling	V_h [m3/s]	0.2131
		V_{max} [m3/s]	0.2138
Mitsubishi FE12NA	Heating	V_h [m3/s]	0.1585
		V_{max} [m3/s]	0.16
Mitsubishi FE12NA	Cooling	V_h [m3/s]	0.1599
		V_{max} [m3/s]	0.16

Table 11 Applicable range of Q/Qmax and V/Vmax for different models

Model	Mode	V/Vmax	Q/Qmax
Fujitsu 12RLS	Heating	0.9236	0.79 - 1.05
		0.7662	0.31 - 0.91
		0.5564	0.22 - 0.72
Fujitsu 12RLS	Cooling	0.9968	0.77 - 1.00
		0.8182	0.34 - 0.71
		0.5997	0.35 - 0.62
Mitsubishi FE12NA	Heating	0.9906	0.19 - 1.00
		0.6795	0.36 - 0.89
		0.4447	0.36 - 0.87
Mitsubishi FE12NA	Cooling	0.9994	0.64 - 1.00
		0.5867	0.25 - 0.84
		0.4267	0.21 - 0.50